efficiency would be determined by varying the hydrocarbon chain length.

In conclusion, saccharide primers such as GlcNAc-C12 and LacNAc-C12 were developed to synthesize neolacto-series oligosaccharides using mammalian cells. The glycosylated products were separated by HPLC, and the sequences were determined by enzymatic digestion and mass spectrometry. The saccharide primers employed in this study are expected to be useful for synthesizing oligosaccharides expressed in mammalian cells.

4. Experimental

4.1. Synthesis of dodecyl 2-acetamido-2-deoxy-β-D-glucopyranoside (GlcNAc-C12)

2-Acetamido-1,3,4,6-tetra-*O*-acetyl-2-deoxy-D-glucopyranoside (Ac_4-GlcNAc) was prepared by reacting *N*-acetylglucosamine (2.5 g, 11.3 nmol, GlcNAc, Sigma) with Ac_2O (15 mL, 159 mmol, Wako Pure Chemicals) in 30 mL of pyridine according to the literature.[19] Ac_4-GlcNAc (3 g, 7.71 mmol) was mixed with TMS-OTf (4.0 mL, 21.9 mmol, E. Merck) in CH_2Cl_2 under nitrogen.[20] The solution was refluxed at 50 °C with stirring for 7 h. After evaporation followed by neutralization with Et_3N, the product was chromatographed on silica gel to examine the progress of the reaction. The reaction mixture was mixed with 1-dodecanol (3.6 mL, 15.5 mmol, Wako Pure Chemicals), $BF_3{\cdot}OEt_2$ (21 mL, 7.9 mmol, Wako Pure Chemicals) in the presence of 4 Å molecular sieves (2.5 g), and stirred at room temperature for 22 h.[21] BF_3-OEt (20.1 mL, 0.79 mmol) was added at 18 h to complete the reaction. The mixture was neutralized with Et_3N. After evaporation, the product was purified by column chromatography (Silica Gel 60, E. Merck, 7 × 30 cm, 1:1 *n*-hexane–EtOAc). Yield: 63.8% (2.53 g). ^{1}H NMR($CDCl_3$): δ 5.51 (d, 1H, $J_{2,NH}$ 8.8 Hz, NH), 5.31 (dd, 1H, $J_{2,3}$ 10.1 Hz, $J_{3,4}$ 9.5 Hz, H-3), 5.06 (dd, 1H, $J_{3,4}$ 9.5 Hz, $J_{4,5}$ 9.9 Hz, H-4), 4.65 (d, 1H, $J_{1,2}$ 8.4 Hz, H-1), 4.26 (dd, 1H, $J_{5,6b}$ 4.7 Hz, $J_{6,gem}$ 12.3 Hz, H-6a), 4.12 (dd, 1H, $J_{5,6a}$ 2.4 Hz, $J_{6,gem}$ 12.3 Hz, H-6b), 3.89–3.75 (m, 2H, $J_{2,NH}$ 8.8 Hz, $J_{1,2}$ 8.4 Hz, H-2, $OCH_2CH_2(CH_2)_9CH_3$), 3.69 (ddd, $J_{4,5}$ 9.9 Hz, $J_{5,6a}$ 2,4 Hz, $J_{5,6b}$ 4.7 Hz, H-5), 3.50–3.42 (m, 1H, $OCH_2CH_2(CH_2)_9CH_3$), 1.94, 2.02, 2.02, and 2.08 (s, each 3H, Ac), 1.60–1.50 (m, 2H, OCH_2CH_2-$(CH_2)_9CH_3$), 1.35–1.14 (m, 18H, $OCH_2CH_2(CH_2)_9CH_3$), 0.87 (t, 3H,$OCH_2CH_2(CH_2)_9CH_3$).

Dodecyl 2-acetamido-3,4,6-tri-*O*-acetyl-2-deoxy-β-D-glucopyranoside (2.5 g, 4.85 mol) in 100 mL of MeOH was deacetylated in the presence of NaOMe (270 mg, 5.0 mmol, Wako Pure Chemicals). Deprotection was carried out with stirring for 40 min. After decolorization on charcoal in EtOH, the product GlcNAc-C12 was obtained by recrystallization in ethanol. Yield: 1.70 g (88.1%). Mp 160–162 °C, lit.[22] mp 161 °C, $[\alpha]_D$ −18.8 (*c* 0.12, CH_3OH). ^{1}H NMR (CD_3OD): δ 4.38 (d, 1H, $J_{1,2}$ 6.1 Hz, H-1), 3.91–3.83 (m, 2H, H-6a, NH), 3.70–3.58 (m, 2H, H-2, H-5), 3.48–3.40 (m, 2H, H-3, H-6b), 3.34–3.27 (m, 3H, H-4, OCH_2), 1.97 (s, 3H, Ac), 1.53–1.51 (m, 2H, $OCH_2CH_2(CH_2)_9CH_3$), 1.34–1.22 (m, 18H, $OCH_2CH_2(CH_2)_9CH_3$), 0.89 (t, 3H, OCH_2CH_2-$(CH_2)_9CH_3$). MALDI-TOFMS: calcd for $C_{20}H_{39}NO_6$: $(M+Na)^+$, 412.3, Found: $(M+Na)^+$, 412.3. Anal. Calcd for $C_{20}H_{39}NO_6{\cdot}0.3H_2O$ (398.68): C, 60.82; H, 10.11; N, 3.55. Found: C, 60.81; H, 10.04; N, 3.54.

4.2. Synthesis of dodecyl β-D-galactopyranosyl-(1→4)-2-acetamido-2-deoxy-β-D-glucopyranoside (LacNAc-C12)

2,3,4,6-Tetra-*O*-acetyl-β-D-galactopyranosyl-(1→4)-2-acetamido-1,3,6-tri-*O*-acetyl-2-deoxy-β-D-glucopyranoside (Ac-LacNAc) was prepared by mixing *N*-acetyllactosamine (982 mg, 2.56 nmol, LacNAc, Yaizu Suisankagaku Industry Co. Ltd, Japan) with Ac_2O (5 mL, 52.9 mmol) in 10 mL of pyridine. Ac-LacNAc (0.799 g, 1.88 mmol) was mixed with TMS-OTf (0.24 mL, 1.33 mmol) in CH_2Cl_2 under nitrogen. The solution was refluxed at 50 °C with stirring for 12 h. After evaporation, followed by neutralization with Et_3N, the product was chromatographed on silica gel to examine the progress of reaction. After evaporation, the product was collected by column chromatography (Silica Gel 60, 2 × 23 cm, 1:2:0.01 toluene–EtOAc–Et_3N). The collected products were mixed with 1-dodecanol (1.3 mL, 5.89 mmol), (*R*,*S*)-camphor sulfonate (27 mg, 0.12 mmol, Wako Pure Chemicals) in the presence of 4 Å molecular sieves (350 mg), and refluxed for 6 h. The mixture was neutralized with Et_3N. After evaporation of the solvent, the product was purified by column chromatography (Silica Gel 60, 2 × 35 cm, 2:3 *n*-hexane–EtOAc). Yield: 50% (478 mg). ^{1}H NMR ($CDCl_3$): δ: 5.63 (d, 1H, $J_{NH,2}$ 9.3 Hz, NH), 5.35 (d, 1H, $J_{3',4'}$ 2.9 Hz, H-4′), 5.11 (dd, 1H, H-2′), 5.06 (dd, 1H, $J_{3,4}$ 8.1 Hz, H-3), 4.97 (dd, 1H, $J_{2',3'}$ 10.3 Hz, H-3′), 4.51–4.46 (m, 2H, H-1′, H-6a), 4.43 (d, 1H, $J_{1,2}$ 7.3, H-1), 4.15–4.09 (m, 3H, H-6b, H-6b′, H-6a′), 4.03 (dd, 1H, $J_{2,3}$ 9.3 Hz, H-2), 3.87 (ddd, 1H, H-5′), 3.78 (dd, 1H, H-4), 3.62 (ddd, 1H, $J_{4,5}$ 5.6 Hz, H-5), 3.41 (dd, 2H, $OCH_2CH_2(CH_2)_9CH_3$), 2.15–1.96 (m, 21H, Ac), 1.60–1.46 (m, 2H, $OCH_2CH_2(CH_2)_9CH_3$), 1.30–1.18 (m, 18H, $OCH_2CH_2(CH_2)_9CH_3$), 0.87 (t, 3H, $OCH_2(CH_2)_{10}CH_3$).

Dodecyl 2,3,4,6-tetra-*O*-acetyl-β-D-galactopyranosyl-(1→4)-2-acetamido-3,6-di-*O*-acetyl-2-deoxy-β-D-glucopyranoside (478 g, 0.56 mmol) in 25 mL of MeOH was deacetylated by the addition of NaOMe (160 mg, 2.97 mmol) with stirring for 3 h. The reactant was concentrated after treating with Amberlite IR-120B (Organo Co., Japan). LacNAc-C12 was purified by distilling with EtOH, toluene, and $CHCl_3$. Yield: 326 mg

(99%). mp 246 °C, $[\alpha]_D$ −7.6 (*c* 0.2, DMSO). ^{1}H NMR(DMSO-d_6): δ 7.74 (d, 1H, NH), 4.28 (d, 1H, $J_{1,2}$ 7.8 Hz, H-1′), 4.19 (d, 1H, $J_{1,2}$ 8.1 Hz, H-1), 1.7 (s, 3H, Ac), 1.42–1.41 (m, 2H, $OCH_2CH_2(CH_2)_9CH_3$), 1.17–1.29 (m, 18H, $OCH_2CH_2(CH_2)_9CH_3$), 0.85 (t, 3H, $OCH_2CH_2(CH_2)_9CH_3$). MALDI-TOFMS: calcd for $C_{26}H_{49}NO_{11}$: $(M+Na)^+$, 574.3, found: $(M+Na)^+$, 574.6. Anal. Calcd for $C_{26}H_{49}NO_{11}\cdot 1.5H_2O$ (578.35): C, 53.96; H, 9.06; N, 2.42. Found: C, 54.24; H, 8.77; N, 2.30.

4.3. Cell culture

HL-60 cells (Riken Cell Bank) were grown in RPMI 1640 medium (Nissui Pharm. Co., Ltd) supplemented with 10% heat-inactivated fetal bovine serum (JRH Biosciences Inc.) at 37 °C in humidified 5% CO_2. B16 cells (Riken Cell Bank) were grown in DMEM (Gibco BRL) supplemented with streptomycin 0.1 g/L, penicillin G potassium 50,000 unit/L, and 10% heat-inactivated fetal bovine serum (JRH Biosciences Inc.) at 37 °C in humidified 5% CO_2.

4.4. Glycosylation of saccharide primers in cells

Stock solutions of 20 mM saccharide primers in DMSO were diluted to 50 μM with serum-free and phenol red-free culture medium consisting of RPMI 1640 medium (Gibco BRL) containing 5 mg/L of transferrin, 5 mg/L of insulin, and 30 nM selenium dioxide.

Glycosylation by cells was carried out as follows: HL60 cells (2×10^6) were incubated with RPMI 1640 medium containing 50 μM saccharide primer for 48 h. The glycosylated products secreted in the culture medium were collected with a Sep-Pak C_{18} column (Waters Co.). The water-soluble compounds were removed with water and 3:7 MeOH–H_2O. The glycosylated products were eluted with MeOH. The eluate containing the glycosylated products was evaporated under reduced pressure. The obtained products were dissolved in 100 μL of 2:1 $CHCl_3$–MeOH, and an aliquot was separated on an HPTLC plate (Silica Gel 60, E. Merck) using $CHCl_3$–MeOH–0.2% $CaCl_2$. Acidic and neutral products on the HPTLC plate were stained with resorcinol–HCl reagent and orcinol–H_2SO_4 reagent, respectively. B16 cells (2×10^6) were similarly incubated with saccharide primers in serum-free DMEM/F-12 medium (Gibco BRL) containing 5 mg/L of transferrin, 5 mg/L of insulin, and 30 nM selenium dioxide.

4.5. TLC blotting

TLC blotting was carried out as follows: Glycosylated products separated on an HPTLC plate were sprayed with primuline reagent, and the spots were marked with a red pencil under UV light. Then, the HPTLC plate was dipped in a blotting solvent of 40:7:20 2-PrOH–MeOH–0.2% $CaCl_2$ for 20 s and placed on a glass fiber filter (ATTO Co.). The plate was covered with a PVDF membrane (ATTO Co.), a PTFE membrane (ATTO Co.), and another glass fiber filter. These layers were subjected to pressure at 180 °C for 30 s using a TLC thermal blotter (ATTO Co.). The PVDF membrane was washed with pure water, and glycolipid fractions were extracted with MeOH and 2:1 $CHCl_3$–MeOH.

4.6. High-performance liquid chromatography (HPLC)

Neutral products and acidic products separated using a Sep-Pak C_{18} column were purified by HPLC. The crude products dissolved in 70:28:2 $CHCl_3$–MeOH–H_2O were injected into an HPLC system equipped with an Iatrobead column (6RSP-8005, 4.6 × 250 mm, Iatron Laboratories Inc.) and a light scattering detector (SEDEX75, Sedere). Neutral products were separated with 70:28:2 $CHCl_3$–MeOH–H_2O. Acidic products were separated with 70:28:2 $CHCl_3$–MeOH–H_2O and 60:35:5 $CHCl_3$–MeOH–H_2O. The flow rate was 2 mL/min. The fractions were collected at 30-s intervals for 40 min.

4.7. Mass spectrometry

The structural analyses of glycosylated products were carried out by a MALDI-TOF mass spectrometer (Autoflex, Bruker Daltonics) and an ESI mass spectrometer (Esquire 3000, Bruker Daltonics). 2,5-Dihydroxybenzoic acid (DHB, Aldrich) was employed as a matrix.

4.8. Digestion of glycosylated products by enzymes

Enzymatic digestion of glycosylated products was carried out in 50 mM NaOAc buffer (pH 4.8) containing 50 mU of neuraminidase from *A. ureafaciens* (EC.3.2.1.18, Sigma), or in 50 mM sodium acetate butter (pH 5.5) containing 10 mU of neuraminidase from *M. decora* (EC. 3.2.1.18, Calbiochem). The reactions were carried out in the presence of 0.6 mg/mL sodium taurodeoxycholic acid. The products were collected using a Sep-Pak C_{18} column, separated on an HPTLC plate with 60:35:8 $CHCl_3$–MeOH–0.2% $CaCl_2$, and were stained with orcinol–H_2SO_4.

4.9. MTT assay

Cells (2×10^4) in a 96-well microplate were incubated with 50 μM GlcNAc-C12 or LacNAc-C12 for 48 h. Ten μL of WST-1 dye solution (10 mM WST-1 and 0.2 mM 1-methoxy PMS, Dojindo Laboratories) per well was added to each well. After 2 h, absorbance at 450 nm with a reference wavelength of 690 nm was measured using a microplate reader (Multiskan, Labsystem).

Acknowledgments

This work was partly supported by funds from the Program for Promotion of Basic Research Activities for Innovative Biosciences, and the Special Coordination of Funds for Promoting Science and Technology from the Ministry of Education, Culture, Sports, Science and Technology, the Japanese Government (T.S.).

Supplementary data

Supplementary data associated with this article can be found, in the online version, at doi:10.1016/j.carres.2008.01.022.

References

1. Miura, Y.; Yamagata, T. *Biochem. Biophys. Res. Commun.* **1997**, *241*, 698–703.
2. Nakajima, H.; Miura, Y.; Yamagata, T. *J. Biochem.* **1998**, *124*, 148–156.
3. Okayama, M.; Kimata, K.; Suzuki, S. *J. Biochem.* **1973**, *74*, 1069–1073.
4. Schwartz, N. B. L.; Galligani, P.-L. Ho.; Dorfman, A. *Proc. Natl. Acad. Sci. U.S.A.* **1974**, *71*, 4047–4051.
5. Sarkar, A. K.; Fritz, T. A.; Taylor, W. H.; Esko, J. D. *Proc. Natl. Acad. Sci. U.S.A.* **1995**, *92*, 3323–3327.
6. Sarkar, A. K.; Rostand, K. S.; Jain, R. K.; Matta, K. L.; Esko, J. D. *J. Biol. Chem.* **1997**, *272*, 25608–25616.
7. Yamagaki, T.; Nakanishi, H. *J. Mass Spectrom.* **2000**, *35*, 1300–1307.
8. Handa, K.; Withers, D.-A.; Hakomori, S. *Biochem. Biophys. Res. Commun.* **1998**, *243*, 199–204.
9. Nishihara, S.; Iwasaki, H.; Kaneko, M.; Tawada, A.; Ito, M.; Narimatsu, H. *FEBS Lett.* **1999**, *462*, 289–294.
10. Saito, M.; Sugano, K.; Nagai, Y. *J. Biol. Chem.* **1979**, *254*, 7845–7854.
11. Chou, M.-Y.; Li, S.-C.; Kiso, M.; Hasegawa, A.; Li, Y.-T. *J. Biol. Chem.* **1994**, *269*, 18821–18826.
12. Pan, G. G.; Melton, L. D. *J. Chromatogr.* **2005**, *1077*, 136–142.
13. Stroud, M.-R.; Holmes, E.-H. *Biochem. Biophys. Res. Commun.* **1997**, *238*, 165–168.
14. Stroud, M.-R.; Handa, K.; Salyan, M.-E.-K.; Ito, K.; Levery, S.-B.; Hakomori, S. *Biochemistry* **1996**, *35*, 758–769.
15. Kasuya, M. C. Z.; Wang, L. X.; Lee, Y. C.; Mitsuki, M.; Nakajima, H.; Miura, Y.; Sato, T.; Hatanaka, K.; Yamagata, S.; Yamagata, T. *Carbohydr. Res.* **2000**, *329*, 755–763.
16. Sato, T.; Fujita, S.; Kasuya, M. C. Z.; Hatanaka, K.; Yamagata, T. *Chem. Lett.* **2004**, *33*, 580–581.
17. Nojiri, H.; Takaku, F.; Tetsuka, T.; Motoyoshi, K.; Miura, Y.; Saito, M. *Blood* **1984**, *64*, 534–541.
18. Sato, T.; Hatanaka, K.; Hashimoto, H.; Yamagata, T. *Trends Glycosci. Glycotechnol.* **2007**, *19*, 1–17.
19. Horton, D. *J. Org. Chem.* **1964**, *29*, 1776–1782.
20. Nakabatashi, S.; Warren, C. D.; Jeanlozs, R. W. *Carbohydr. Res.* **1986**, *150*, C7–C10.
21. Xia, J.; Piskorz, C. F.; Locke, R. D.; Chandrasekaran, E. V.; Alderfer, J. L.; Matta, K. L. *Bioorg. Med. Chem. Lett.* **1999**, *9*, 2941–294622.
22. Boullanger, P.; Chevalier, Y.; Croizier, M.-C.; Lafont, D.; Sancho, M.-R. *Carbohydr. Res.* **1995**, *278*, 91–101.

Selection of a Carbohydrate-Binding Domain with a Helix−Loop−Helix Structure[†]

Teruhiko Matsubara,[‡] Mie Iida,[‡] Takeshi Tsumuraya,[§] Ikuo Fujii,[§] and Toshinori Sato*[,‡]

Department of Biosciences and Informatics, Faculty of Science and Technology, Keio University, 3-14-1 Hiyoshi, Kouhoku-ku, Yokohama 223-8522, Japan, and Department of Biological Science, Graduate School of Science, Osaka Prefecture University, 1-2 Gakuen-cho, Sakai, Osaka 599-8570, Japan

Received January 16, 2008; Revised Manuscript Received March 19, 2008

ABSTRACT: We obtained a novel carbohydrate-binding peptide having a helix−loop−helix scaffold from a random peptide library. The helix−loop−helix peptide library randomized at five amino acid residues was displayed on the major coat protein of a filamentous phage. Affinity selection with a ganglioside, Galβ1−3GalNAcβ1−4(Neu5Acα2−3)Galβ1−4Glcβ1−1′Cer (GM1), gave positive phage clones. Surface plasmon resonance spectroscopy showed that a corresponding 35-mer synthetic peptide had high affinity for GM1 with a dissociation constant of 0.24 μM. This peptide preferentially binds to GM1 rather than asialo GM1 and GM2, suggesting that a terminal galactose and sialic acid are required for the binding as for cholera toxin. Circular dichroism spectroscopic studies indicated that a helical structure is important for the affinity and specificity. Furthermore, alanine scanning at randomized positions showed that arginine and phenylalanine play an especially important role in the recognition of carbohydrates. Such a de novo helix−loop−helix peptide would be available for the design of carbohydrate-binding proteins.

Lectins, antibodies, and proteins which are specific to carbohydrates serve as powerful tools in the identification of the physiological roles of glycoconjugates (*1*). Despite this, because glycotopes are poor immunogens, it is difficult to obtain antiglycan and antiglycolipid antibodies (*2*, *3*). Approximately two-thirds of carbohydrate-binding antibodies are IgM (*2*), their affinity and specificity not always being sufficient in clinical use as a glycan probe. To overcome this, the affinity of antibodies has been improved through selection from phage-display libraries over the past decade (*4*). The affinity of monoclonal antibodies against oligosaccharides of Lewis^X (*5*), sialyl Lewis^X (*6*), α-galactosyl epitope (*7*), Thomsen-Friedenreich antigen (*8*), Galβ1−3GalNAcβ1−4Galβ1−4Glcβ1−1′Cer (asialo GM1)[1] (*3*), and Neu5Gcα2−3Galβ1−4Glcβ1−1′Cer (*N*-glycoyl GM3) (*9*) has improved. When it comes to lectin (*10*, *11*) and hemagglutinin (*12*, *13*), attempts to change binding specificity through mutation have been reported.

An alternative strategy might have great potential in the engineering of tailor-made artificial carbohydrate-binding proteins. Research groups have adopted various structural motifs for the de novo design of polypeptides such as metalloproteins (*14*), catalysts (*15*, *16*), and bacteriorhodopsin (*17*). Random library-based selection and evolution with structural scaffolds using display technologies have provided proteins that target specific molecules (*18*, *19*). In this study, a stable helix−loop−helix structure was chosen to construct an artificial carbohydrate-binding domain. Helix-based motifs are frequently conserved in proteins during molecular evolution (*20*). Selection from a randomized peptide library with the helix-type scaffold would give peptides that play a role as a carbohydrate-binding domain.

The ganglioside GM1 is well-known as a receptor of cholera toxin B subunit (CTB) (*21*, *22*) and is often used as a marker of lipid rafts (*23*). Yanagisawa noted that GM1 is correlated with the accumulation of β-amyloid in cases of Alzheimer's disease (*24*). The development of GM1-binding molecules is required for investigation of the localization and roles of GM1 on the cell surface. Our previous selection from a random library showed a pentadecapeptide, p3, with affinity for a GM1 pentasaccharide with a dissociation constant (K_d) of 1.2 μM (*25*, *26*). This peptide was specific to GM1 as well as CTB, but the binding affinity of the peptide was lower than that of CTB ($K_d = 10^{-8}$–10^{-12} M) (*22*). Two-dimensional nuclear magnetic resonance (NMR) experiments showed that a conformational change of this peptide occurred during the binding to GM1 (*27*). To decrease the entropic loss caused by the conformational change, a helix-type scaffold was adopted for the selection. Five amino acids at the C-terminal helix of the helix−loop−helix scaffold were randomized to identify the GM1-specific peptide sequences. Phage display selection, alanine scanning, and circular dichroism experiments indicated the peptide to be specific

[†] This work was supported by a Grant-in-aid for the Encouragement of Young Scientists (17750166, T.M.) from the Ministry of Education, Culture, Sports, Science and Technology of the Japanese Government.

* To whom correspondence should be addressed: Department of Biosciences and Informatics, Faculty of Science and Technology, Keio University, 3-14-1 Hiyoshi, Kouhoku-ku, Yokohama 223-8522, Japan. Phone: +81-45-566-1771. Fax: +81-45-566-1447. E-mail: sato@bio.keio.ac.jp.

[‡] Keio University.

[§] Osaka Prefecture University.

[1] Abbreviations: GSL, glycosphingolipid; GM1, Galβ1−3GalNAcβ1−4(Neu5Acα2−3)Galβ1−4Glcβ1−1′Cer; GM2, GalNAcβ1−4(Neu5Acα2−3)Galβ1−4Glcβ1−1′Cer; asialo GM1, Galβ1−3GalNAcβ1−4Galβ1−4Glcβ1−1′Cer; GlcCer, Glcβ1−1′Cer; CTB, cholera toxin B subunit; K_d, dissociation constant; NMR, nuclear magnetic resonance; CFU, colony-forming units; PBS, phosphate-buffered saline; TBS, Tris-buffered saline; BSA, bovine serum albumin; ELISA, enzyme-linked immunosorbent assay; CD, circular dichroism; SPR, surface plasmon resonance; RU, resonance units; R_{max}, maximum resonance; R_{eq}, equilibrium resonance units; ΔG, Gibbs free energy change.

10.1021/bi8000837 CCC: $40.75
Published on Web 06/10/2008

to GM1 and the helical conformation to be necessary for the specific binding.

EXPERIMENTAL PROCEDURES

Materials. Gangliosides and glycosphingolipids (GSLs), Galβ1−3GalNAcβ1−4(Neu5Acα2−3)Galβ1−4Glcβ1−1′Cer (GM1), GalNAcβ1−4(Neu5Acα2−3)Galβ1−4Glcβ1−1′Cer (GM2), Galβ1−3GalNAcβ1−4Galβ1−4Glcβ1−1′Cer (asialo GM1), and Glcβ1−1′Cer (GlcCer) were obtained from Sigma-Aldrich Co. (St. Louis, MO). Anti-fd bacteriophage antibody, peroxidase-conjugated anti-rabbit IgG antibody, and peroxidase-conjugated cholera toxin B subunit (CTB) were obtained from Sigma-Aldrich. XL1-blue cell and helper phage (VCSM13) were obtained from Stratagene Co. (La Jolla, CA).

Phage Display Library. A random library of a helix−loop−helix peptide, AELAALEAELAALE-G_7-KLXXLKXKLXX-LKA, was constructed using a pComb8 system (*28*). This library was displayed on major coat protein VIII of a filamentous phage with a GGSSA spacer and GAPVPYP-DPLEPR (E-tag). We estimated the library has 3.2×10^7 recombinants, which is enough diversity to cover five randomized amino acids ($20^5 = 3.2 \times 10^6$).

Affinity Selection with GM1. For affinity selection, a ganglioside GM1 monolayer was prepared at the air−water interface in a Langmuir trough and immobilized onto a plastic plate (code 174950, Nunc) as reported previously with a minor modification (*25*, *26*). The phage library (5×10^9 CFU) was incubated with GM1 in 200 μL of phosphate-buffered saline (PBS) at pH 6.0 ([phage] = 0.041 nM). After 30 min, the GM1 plate was washed three times to remove unbound phages. Bound phages were eluted for 15 min with glycine-HCl buffer (pH 2), and the eluate was neutralized with Tris-HCl buffer at pH 9.1. To estimate the phage number collected, a small portion of the eluate was saved and used for titering. *Escherichia coli* XL1-blue cells were infected with the phages in SB medium incubated for 30 min at 37 °C. After the addition of ampicillin, the transformed cells were grown for 1 h at 37 °C. The phages were rescued by adding a VCSM13 helper phage and further amplified overnight. The phages amplified were collected and purified with polyethylene glycol and NaCl for the next round. This process was repeated seven or nine times. After the last round of affinity selection, the titering plate was used to isolate individual phage clones. Each phagemid cloned was purified with a QIAprep Spin Miniprep Kit (QIAGEN Inc.) and used as a template for sequencing to deduce the amino acid sequence.

Peptide Synthesis and Purification. Peptides (peptide amides) were synthesized with a solid-phase peptide synthesizer (model 433A, Applied Biosystems) using 9-fluorenylmethoxycarbonyl (Fmoc) chemistry. The peptides were purified by reversed-phase high-performance liquid chromatography (C_{18} column, 250 mm × 20 mm inside diameter) with a linear gradient of water containing 0.1% trifluoroacetic acid (TFA) and acetonitrile containing 0.1% TFA at a flow rate of 10 mL/min. The major fractions were lyophilized, and the peptides were characterized by matrix-assisted laser desorption ionization time-of-flight mass spectrometry (autoflex, Bruker Daltonics, Inc.) using a matrix of α-cyano-4-hydroxycinnamic acid.

Circular Dichroism (CD) Spectroscopy. CD spectroscopy was performed on a Jasco J-820 spectropolarimeter using a 1 mm cuvette. Spectra were collected from 260 to 190 nm every 0.2 nm. The peptide concentrations were determined by measuring tyrosine absorbance (the molar absorbance coefficient at 257 nm equals 1450 M^{-1} cm^{-1}). A peptide solution (100 μM) was prepared with Tris-buffered saline (TBS) (50 mM Tris-HCl and 150 mM NaCl) at pH 7.5. The CD spectra are reported as mean residue ellipticity ([θ]) in degrees per square centimeter per decimole. The α-helical content was calculated from the following equation (*29*).

$$\alpha\text{-helical content} = (-[\theta]_{222} + 2340)/30300$$

Surface Plasmon Resonance (SPR) Analysis. The affinity of peptides for glycolipids was determined by SPR using a Biacore X biosensor system (Biacore International). The glycolipid monolayer was immobilized on a bare gold sensor chip (code BR-1004-05, Biacore International), and this chip was docked into the instrument. All measurements were carried out in TBS (pH 7.5) which was filtered (0.22 μm) and degassed prior to use. After the docking, TBS was injected over the chip at a flow rate of 10 μL/min for 30−40 min. Analyses were performed at 25 °C and with a flow rate of 5 μL/min for the determination of equilibrium binding. The sensor chip surfaces were regenerated with 4 M $MgCl_2$ for 8 min.

Binding affinity was calculated from a Scatchard analysis of equilibrium binding using the equation

$$R_{eq}/[\text{peptide}] = R_{max}/K_d - R_{eq}/K_d$$

where [peptide], R_{max}, and K_d are the concentration of peptide, the maximum resonance, and the dissociation constant, respectively. The resonances in the association phase at 500−600 s were used as the equilibrium resonance units (R_{eq}). The average R_{eq} values were plotted in the form R_{eq}/[peptide] versus R_{eq}, and K_d and R_{max} were calculated from the slope and intercept of the linear relationship, respectively. The peptide concentration range (1−20 μM) in which the peptide amounts were analyzed as a single interaction by a Scatchard plot was used to determine K_d values. In the case of B72, the concentrations of 1−10 μM were used for the analysis, since the multilayer adsorption was observed at 20 μM and reliable signals were not detected below 1 μM.

Molecular Modeling. Molecular modeling was performed using the InsightII/Discover3 system (Accelrys, Inc.). The peptide amide Ct5 was built using the Biopolymer module in InsightII, where the main chains of 1−14 and 22−36 residues are taken as the helical structure and the chain of 15−21 residues is extended. Simple minimization was performed using Discover3. To obtain peptide B72, substitutions of four alanines with Lys24, Arg28, Arg31, and Phe32 were made in Ct5 using the Biopolymer module. After the minimization, the final structure was used for the drawing shown in Figure 8. Crystallographic coordinates of the X-ray structure of pentasaccharide GM1 were obtained from the Protein Data Bank (entry 3CHB). The B72 peptide and GM1 pentasaccharide were superimposed.

RESULTS

Helix−Loop−Helix Design. The helix−loop−helix scaffold is composed of two helical sequences with seven

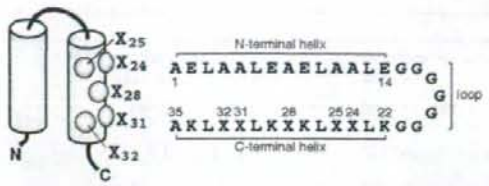

FIGURE 1: Structure of the helix−loop−helix library. An illustration of the helix−loop−helix library is shown at the left. Five randomized positions are arranged in the C-terminal helix, where X is a randomized position. The amino acid sequence of the helix−loop−helix peptide library is shown at the right.

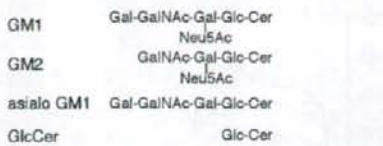

FIGURE 2: Schematic representation of gangliosides and GSLs employed in this study. Glc, glucose; Gal, galactose; GalNAc, *N*-acetylgalactosamine; Neu5Ac, *N*-acetylneuraminic acid; Cer, ceramide.

glycines as a spacer (Figure 1) (*30*). Leucines, glutamic acids, and lysines were positioned to stabilize the helical structure through hydrophobic interaction and the formation of salt bridges. We prepared a helix−loop−helix library for phage display selection with random substitutions at positions 24, 25, 28, 31, and 32 (*31*). The substituted residues were positioned outside of the C-terminal helix.

Phage Display Selection against GM1. The selection of peptides with affinity for ganglioside GM1 (Figure 2) was carried out as reported with minor revisions (*25*). Briefly, a GM1 monolayer was prepared at the air−water interface with a Langmuir trough and transferred to a plastic plate. The phage library was incubated with GM1 on the plate, and the bound phages were eluted under acid conditions. The phages obtained were amplified, purified, and subjected to another round. After seven and nine rounds of selection, 16 and 20 clones were isolated, respectively. The phage ELISA was used to identify the clones that have affinity for GM1 (Supporting Information, Figure S1). The first screening of 36 phage clones was performed via an ELISA, and then 13 clones were chosen for further investigation. To know the binding selectivity of 13 clones, K_d values for GM3 and GalCer were also investigated (data not shown). A914 and B72 were found to have high affinity for GM1 with K_d values of 0.075 and 0.13 nM, respectively, and exhibited a higher affinity than for GM3 and GalCer (Supporting Information, Table S1).

Binding Affinity and Helical Structure of Peptides. To analyze their affinity, these peptides were chemically synthesized (C-terminus amidated). To estimate the peptide concentration in buffer, tyrosine was added at the C-terminus of the peptide (Table 1). The binding of these peptides was characterized by the surface plasmon resonance method. Figure 3A shows typical sensorgrams of peptides A914, B72, and Ct5 at 10 μM in TBS (pH 7.5). Ct5 is a control peptide in which all sites randomized in the library are changed to alanines. The amount of B72 bound to GM1 was greater than that of other peptides and increased as the peptide concentration increased (Figure 3B). However, the kinetics of binding was not analyzed due to the rapid association and dissociation phases observed. Then, equilibrium binding experiments were performed to calculate K_d values using Scatchard plots; the K_d was 2.9 μM for A914, 0.24 μM for B72, and 11 μM for Ct5 (Table 1 and Figure 4). The binding affinity of B72 was 25-fold higher than that of the control Ct5. The R_{max} values for B72, Ct5, and B72-h, which is the C-terminal half of B72 containing five residues identified, were 280, 268, and 145 RU, respectively. These amounts bound to GM1 approximately corresponded to their molecular weights. However, A914 showed low affinity (2.9 μM) and small amounts (151 RU) against GM1, though the A914 phage clone had the same affinity for GM1 as the B72 clone (Table S1). Such a discrepancy between synthetic peptides and phage clones is often observed (*25*, *32*). The binding preference of the selected peptides depends on the method of measurement. Then, on the basis of the results in Table 1, we chose B72 for further characterization. The K_d value of a 15-mer peptide, p3, selected previously was 1.2 μM (*26*). B72 exhibited greater (5-fold) affinity for GM1 than the nonhelical peptide p3. Lectins, toxins, and antibodies have several carbohydrate-binding domains (*33*). A multivalent B72 as tandem repeats or tentacle-type multimers would enhance the binding affinity (*34*).

To clarify how the helix of B72 is affected upon carbohydrate recognition, the secondary structure of B72 was investigated by CD spectroscopy. The CD spectra of B72 and Ct5 exhibited two minima at 208 and 222 nm, indicating a typical α-helical structure (Figure 5) (*35*). The mean residue ellipticity at 222 nm was −10471 deg cm^2 dmol^{-1} for B72 and −16040 deg cm^2 dmol^{-1} for Ct5. The helical content was estimated to be 42% for B72 and 61% for Ct5 (*29*). B72-h took no helical structure and had a lower affinity (K_d = 5.0 μM) than full-length B72 (K_d = 0.24 μM) (Table 1). These results suggest that the binding of B72 to GM1 was influenced by its secondary structure.

Binding Specificity of Peptides. The specificity with which B72, Ct5, and B72-h bind various glycolipids is shown in Figure 6 and summarized in Table 2. The affinity of B72 was 0.016- and 0.073-fold lower for GM2 and asialo GM1 than for GM1, respectively (15 μM for GM2 and 3.3 μM for asialo GM1). The binding preference (GM1 ≫ asialo GM1 > GM2) of B72 was in good agreement with that of p3 (*26*). The profile of the binding of Ct5 to GM1 was no different from that of the binding to other glycolipids, and the amount of B72-h bound to GM1 declined to the same level as that bound to GlcCer (as nonspecific binding) (Figure 6). These results suggested that the helical conformation and the five residues in B72 were crucial for the specificity for GM1.

Alanine Scanning. To determine the contribution of the five residues in B72, four alanine-substituted mutants of B72 were synthesized (B72-1, B72-2, B72-3, and B72-4) (Table 3). Single-alanine substitutions at positions 24, 28, 31, and 32 are predicted to alter the GM1 binding profile and helical conformation. The amount of peptide bound to GM1 was affected by all alanine substitutions (Table 3, Figure 7A, and Figure S2). Notably, the replacement of Arg31 (B72-3) and Phe32 (B72-4) with Ala markedly decreases the affinity for GM1; the amounts of B72-3 (67 RU at 5 μM) and B72-4 (54 RU) were 4−5-fold smaller than the amount of B72 (261 RU). The amounts of these mutants decreased to the same level as the control peptide, Ct5 (80 ± 23 RU at 5 μM) (Figure 6). It was suggested that Arg31 and Phe32 among

Table 1: Affinity of Synthetic Peptides for GM1

code	peptide structure [a]	molecular weight	R_{max} (RU)	K_d (μM)	relative affinity [b]
A914	AELAALEAELAALEGGGGGGGKLQELKTKLAALKAY-NH_2	3512.02	151	2.9	0.083
B72	AELAALEAELAALEGGGGGGGKLKALKRKLRFLKAY-NH_2	3670.31	280	0.24	1.0
B72-h	GGGKLKALKRKLRFLKAY-NH_2	1743.14	145	5.0	0.048
Ct5	AELAALEAELAALEGGGGGGGKLAALKAKLAALKAY-NH_2	3366.90	268	11	0.022

[a] Random positions are underlined. [b] Ratio to B72 peptide.

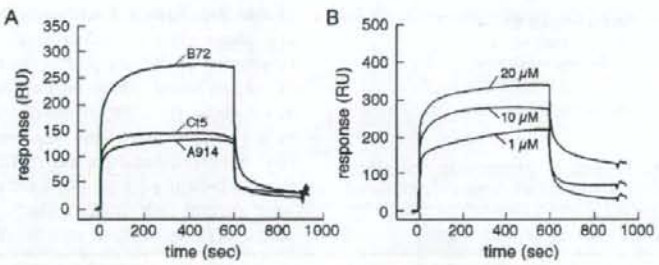

FIGURE 3: SPR sensorgrams for the interaction of peptides with GM1. (A) Overlay plot of the binding of A914, B72, and Ct5 at 10 μM. (B) Overlay plot of the binding of B72 at 1, 10, and 20 μM. Responses in RU are plotted vs time in seconds. Association (0−600 s) and dissociation (600−900 s) phases are shown.

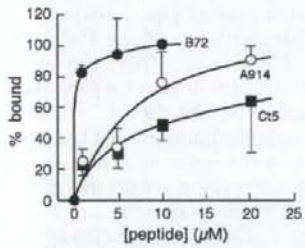

FIGURE 4: Amounts of A914, B72, and Ct5 bound to GM1 at various peptide concentrations observed by SPR spectroscopy. % bound, $(R_{eq}/R_{max}) \times 100$; R_{eq}, equilibrium response units at 500−600 s in the association phase; R_{max}, maximum response calculated from Scatchard plots (data not shown). The data are average values ± the standard deviation ($n = 2-4$).

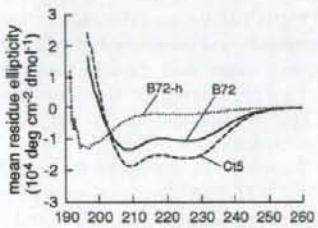

FIGURE 5: CD spectra of B72 (—), B72-h (•••), and Ct5 (---) in TBS at pH 7.5. The peptide concentration was 100 μM.

the four amino acid residues strongly contributed to the binding. In our previous studies, arginines and hydrophobic amino acids had been found in the motif shared among GM1-binding peptides (*25, 26*). These results were consistent with our previous papers.

To determine the influence of alanine substitutions on the helical conformation, CD spectra of these mutants were measured (Figure 7B). The two maxima at 208 and 222 nm were found in all the mutants, which indicates that the helical structure was maintained. The mean residue ellipticity at 222 nm of B72 mutants decreased except for that of B72-2; indeed, the α-helical content increased (65, 34, 59, and 48% for B72-1, B72-2, B72-3, and B72-4, respectively). Alanine is a stabilizer of helices, so an enhancement of helicity with alanine substitutions is reasonable (*36*). The CD spectra indicated that the decreases in affinity for GM1 are due to the loss of side chains of residues identified, and not due to disruption of the helical conformation.

DISCUSSION

The development of carbohydrate-binding molecules like lectins, toxins, and antibodies would greatly contribute to the evolution of glycoscience and glycotechnology. Especially for functional analyses of glycoconjugates, the need for carbohydrate-binding molecules will increase with progress in glycobiology (*37−41*). Recently developed selection technology, including the use of genomic and random libraries, has provided various repertories of carbohydrate-binding molecules (*42*). Lectin mutations, antibody libraries, and peptide libraries are beneficial sources. We have so far identified carbohydrate-binding molecules, regardless of natural sequences. We previously identified GM1-binding pentadecapeptides (15-mer peptides) from a random peptide library, one of which, p3, was specific to GM1 with a K_d of 1.2 μM (*25, 26*). This peptide exhibited unique recognition, including specific binding of the high-density GM1 domain. NMR analyses indicated that p3 underwent a conformational change on binding to GM1 (induced fit) (*27*). N-Terminal and C-terminal residues of p3 are flexible in the free state but are restricted once the carbohydrate−peptide interaction occurs. The energy of this binding could be used to overcome the entropy cost for this change. If the peptide conformation is rigid, no binding energy would have to be expended to pay the cost of this folding. We

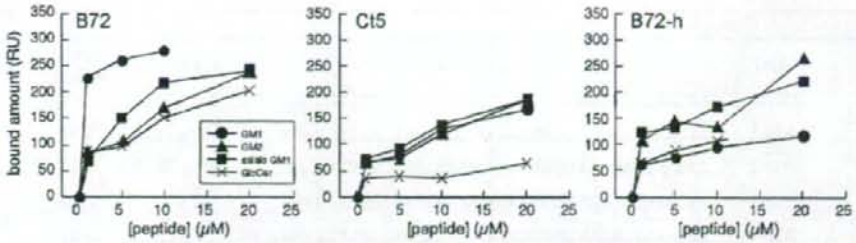

FIGURE 6: Amounts of B72, Ct5, and B72-h peptides bound to gangliosides and GSLs observed by SPR spectroscopy.

Table 2: Affinity of Synthetic Peptides for GM1, GM2, Asialo GM1, and GlcCer

peptide	glycolipid	R_{max} (RU)	K_d (μM)	relative affinity[a]
B72	GM1	280	0.24	1.0
	GM2	418	15	0.016
	asialo GM1	278	3.3	0.073
	GlcCer	322	12	0.020
Ct5	GM1	268	11	1.0
	GM2	377	21	0.52
	asialo GM1	275	9.9	1.1
	GlcCer	nd[b]	nd[b]	nd[b]
B72-h	GM1	145	5.0	1.0
	GM2	274	2.1	2.4
	asialo GM1	285	5.9	0.85
	GlcCer	110	0.77	6.5

[a] Ratio to GM1. [b] Not detectable.

therefore designed a novel carbohydrate-binding peptide with a structural scaffold in this study.

A helical conformation is the only structure that we can design. A helix−loop−helix (or helix−turn−helix) scaffold allows a peptide to form a stable helical structure. Fujii et al. designed a helix−loop−helix peptide library; the helix outside of five residues at 24, 25, 28, 31, and 32 was randomized to give a peptide library (*31*). The N-terminal residues interact with the C-terminus to stabilize the α-helical structure; therefore, this peptide is a monomer and does not form a dimer. They previously identified peptide agonists of the cytokine receptor and granulocyte colony-stimulating factor receptor using helix−loop−helix libraries (unpublished data). In this study, we conferred the ability to recognize carbohydrates on this peptide. The selection procedure followed that previously reported by us; a glycolipid monolayer was immobilized onto a plate and incubated with the phage library (*25*). This method allows the suppression of nonspecific interaction of phage particles with the lipid portion of the glycolipid and the plate surface exposed. The phage particles therefore interact with only the exposed carbohydrate portion of the glycolipid. The two GM1-positive clones, A914 and B72, were identified via a phage ELISA and were chemically synthesized. A synthetic B72 peptide showed specific binding to GM1 with a K_d of 0.24 μM and was found to have the highest affinity for GM1 as suggested by the phage ELISA (Table 1). The K_d value of Ct5, as a control peptide, was 11 μM, and Ct5 exhibited no specificity (Table 2 and Figure 6). This is because the helix−loop−helix scaffold contains several charged amino acids, glutamic acids (positions 2, 7, 9, and 14), and lysines (positions 22, 27, 29, and 34). These amino acids are able to interact nonspecifically with carbohydrates through hydrogen binding and/or salt bridges. These nonspecific interactions contributed to the binding affinity but were not involved directly in the specific interaction between the peptide and GM1 oligosaccharide. Therefore, the five amino acids, Lys24, Ala25, Arg28, Arg31, and Phe31, would be very important for the specific recognition of GM1. Furthermore, to determine whether formation of a helix is essential for binding, we designed a B72-h peptide that is the 18 C-terminal residues containing the five amino acids. The CD spectrum of B72-h exhibited an unordered structure (Figure 5). The five amino acid residues are therefore randomly arranged, and the orientation of these side chains would not be restricted. As expected, B72-h lost affinity and selectivity for GM1 (K_d = 5.0 μM) (Table 2 and Figure 6). These results indicate that the helical conformation of B72 is essential for the recognition of GM1.

Next, alanine-substituted mutants of B72 were used to identify the contributions of the selected amino acid residues to the binding to GM1. CD spectra indicated that replacing Lys24, Arg31, and Phe32 with alanine in the B72 peptide did not affect the helical conformation (Figure 7B). The substitution of Arg31 and Phe32 with alanine drastically changed the affinity (Figure 7A and Table 3), which indicates that these residues are essential for GM1's recognition. These residues would be arranged in the C-terminal helix (Figure 1). We previously identified the GM1-binding motif, (W/F)RxL(xP/Px)xFxx(Rx/xR)xP, and the binding of p3 mutants also showed that Arg and hydrophobic residues (Trp and Phe) contributed to the binding (*26*). Polar and aromatic amino acids often play important roles at carbohydrate-binding sites, because carbohydrate−protein interaction is achieved by a combination of hydrophobic interaction and hydrogen bonding (*33*, *43*). The results of alanine scanning were well consistent with our previous results (*26*).

To estimate how much these five amino acids and the helical conformation contribute to formation of the B72−GM1 complex, the Gibbs free energy change (ΔG) upon formation of the complex was calculated from the K_d values. The ΔG values were calculated using the equation $\Delta G = -RT \ln K_d$, where T = 298 K. The difference in ΔG values between the Ct5−GM1 complex (−28.3 kJ/mol) and the B72−GM1 complex (−37.8 kJ/mol) was 9.5 kJ/mol (Figure 8). This energy difference is thought to be due to the five residues, because the only difference between the B72 and Ct5 sequences is these residues. Since the ΔG value of the B72-h−GM1 complex was −30.2 kJ/mol, the distribution of the helical conformation with the presence of the N-terminal half might be estimated to be 7.5 kJ/mol. These energy differences, 9.5 and 7.5 kJ/mol, suggest that both the five residues and the helical conformation were required for the suitable spatial arrangement of five residues on the helix to achieve the specific B72−GM1 interaction.

Table 3: Amounts of Synthetic Peptides Bound to GM1

code	peptide structure [a]	R_{eq} (RU) [b]	relative amount [c]
B72	AELAALEAELAALEGGGGGGGKLKALKRKLRFLKAY-NH_2	261 ± 69	1.0
B72-1	AELAALEAELAALEGGGGGGGKL<u>A</u>ALKRKLRFLKAY-NH_2	130 ± 21	0.50
B72-2	AELAALEAELAALEGGGGGGGKLKAL<u>A</u>KLRFLKAY-NH_2	97 ± 38	0.37
B72-3	AELAALEAELAALEGGGGGGGKLKALKRKL<u>A</u>FLKAY-NH_2	67 ± 3	0.26
B72-4	AELAALEAELAALEGGGGGGGKLKALKRKLR<u>A</u>LKAY-NH_2	54 ± 15	0.21

[a] Alanine substitutions are underlined. [b] The peptide concentration is 5 μM. [c] Ratio to B72.

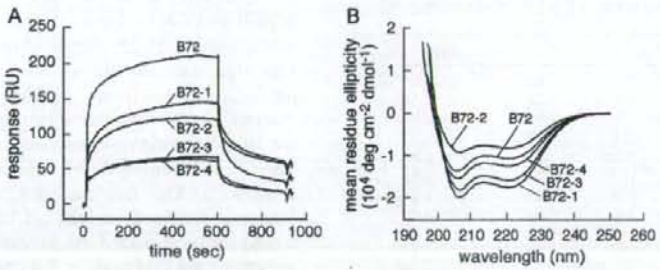

FIGURE 7: Effect of alanine substitutions on the binding of B72 to GM1 and helix formation. (A) SPR sensorgrams for the interaction of B72 and B72 mutants at 10 μM with GM1. (B) CD spectra of B72 and B72 mutants in TBS at pH 7.5. The peptide concentration was 100 μM.

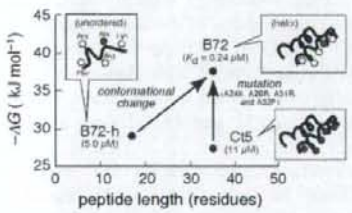

FIGURE 8: Changes in the Gibbs free energy between the complexes of B72, B72-h, and Ct5 with GM1. The ΔG value was calculated from the equation $\Delta G = -RT \ln K_d$, where $T = 298$ K.

B72 exhibited a decrease in the amount bound to asialo GM1 and GM2 (Figure 6), which means that a terminal Gal and Neu5Ac of GM1 are required for the interaction. CTB and p3 also bind to the terminal Gal and Neu5Ac of GM1 (*21*, *22*, *26*). X-ray structural data for the CTB−GM1 complex (Protein Data Bank entry 3CHB) show that the terminal Gal and Neu5Ac interacted with CTB. Therefore, these sugar residues are expected to interact with p3 or B72 in a similar manner. In fact, the binding of CTB to GM1 was competitively replaced with that of B72, and the concentration required for 50% inhibition was 1.1 μM (Supporting Information, Figure S3) (*26*). The molecular modeling shown in Figure 9 indicated that Lys24, Arg28, Arg31, and Phe32 in the C-terminal helix of B72 are arranged to interact with the terminal Gal and Neu5Ac in GM1. A guanidinium group of Arg can form a hydrogen bond with an OH group of the terminal Gal or Neu5Ac and/or salt bridge with a carboxyl group of Neu5Ac. The phenyl group of Phe can form a stack with the hydrophobic B face of the terminal Gal and/or acetoamido group of Neu5Ac.

In conclusion, oligosaccharide-binding peptides with a helix−loop−helix scaffold were selected and their specificities were investigated. One of the peptides exhibited an

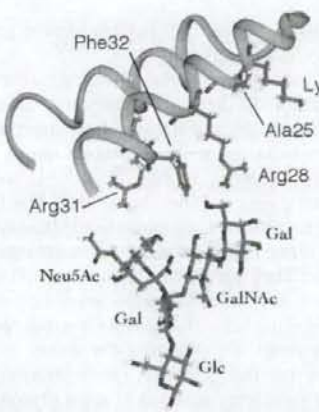

FIGURE 9: Deduced model for the interaction between B72 and pentasaccharide GM1. The side chains of Lys24, Ala25, Arg28, Arg31, and Phe32 in B72 are shown in a stick representation. The GM1 pentasaccharide structure was obtained from Protein Data Bank entry 3CHB.

increase in binding affinity compared with a 15-mer peptide that we identified previously (*26*). The new peptide's helical structure contributed to its ability to recognize carbohydrates, and arginine and phenylalanine were found to be involved in its interaction with GM1. The GM1-binding amino acid residues in the α-helix enabled the peptide to fit GM1. Many antibodies and lectins achieve greater affinity for carbohydrates by displaying carbohydrate-binding residues with a structural scaffold (*33*). This is the first paper to demonstrate the advantages of the arrangement of carbohydrate-binding residues in the helix−loop−helix scaffold for increasing binding affinity.

ACKNOWLEDGMENT

We thank Prof. H. Yanagawa and Dr. N. Doi (Keio University) for providing the opportunity to use the CD spectrometer.

SUPPORTING INFORMATION AVAILABLE

A saturation binding curve of phages to GM1 determined via an ELISA (Figure S1), affinity of phages for various glycolipids (Table S1), amounts of B72 mutant peptides bound to GM1 (Figure S2), and competitive inhibition assay of peptides (Figure S3). This material is available free of charge via the Internet at http://pubs.acs.org.

REFERENCES

1. Varki, A. (1993) Biological roles of oligosaccharides: All of the theories are correct. *Glycobiology 3*, 97–130.
2. Kannagi, R., and Hakomori, S. (2001) A guide to monoclonal antibodies directed to glycotopes. *Adv. Exp. Med. Biol. 491*, 587–630.
3. Qiu, J. X., Kai, M., Padlan, E. A., and Marcus, D. M. (1999) Structure-function studies of an anti-asialo GM1 antibody obtained from a phage display library. *J. Neuroimmunol. 97*, 172–181.
4. Bradbury, A. R., and Marks, J. D. (2004) Antibodies from phage antibody libraries. *J. Immunol. Methods 290*, 29–49.
5. Dinh, Q., Weng, N. P., Kiso, M., Ishida, H., Hasegawa, A., and Marcus, D. M. (1996) High affinity antibodies against Le^b and sialyl Le^x from a phage display library. *J. Immunol. 157*, 732–738.
6. Mao, S., Gao, C., Lo, C. H., Wirsching, P., Wong, C. H., and Janda, K. D. (1999) Phage-display library selection of high-affinity human single-chain antibodies to tumor-associated carbohydrate antigens sialyl $Lewis^x$ and $Lewis^x$. *Proc. Natl. Acad. Sci. U.S.A. 96*, 6953–6958.
7. Wang, L., Radic, M. Z., Siegel, D., Chang, T., Bracy, J., and Galili, U. (1997) Cloning of anti-Gal Fabs from combinatorial phage display libraries: Structural analysis and comparison of Fab expression in pComb3H and pComb8 phage. *Mol. Immunol. 34*, 609–618.
8. Ravn, P., Danielczyk, A., Jensen, K. B., Kristensen, P., Christensen, P. A., Larsen, M., Karsten, U., and Goletz, S. (2004) Multivalent scFv display of phagemid repertoires for the selection of carbohydrate-specific antibodies and its application to the Thomsen-Friedenreich antigen. *J. Mol. Biol. 343*, 985–996.
9. Rojas, G., Talavera, A., Munoz, Y., Rengifo, E., Krengel, U., Angstrom, J., Gavilondo, J., and Moreno, E. (2004) Light-chain shuffling results in successful phage display selection of functional prokaryotic-expressed antibody fragments to N-glycolyl GM3 ganglioside. *J. Immunol. Methods 293*, 71–83.
10. Yamamoto, K., Maruyama, I. N., and Osawa, T. (2000) Cyborg lectins: Novel leguminous lectins with unique specificities. *J. Biochem. 127*, 137–142.
11. Yim, M., Ono, T., and Irimura, T. (2001) Mutated plant lectin library useful to identify different cells. *Proc. Natl. Acad. Sci. U.S.A. 98*, 2222–2225.
12. Yamada, S., Suzuki, Y., Suzuki, T., Le, M. Q., Nidom, C. A., Sakai-Tagawa, Y., Muramoto, Y., Ito, M., Kiso, M., Horimoto, T., Shinya, K., Sawada, T., Usui, T., Murata, T., Lin, Y., Hay, A., Haire, L. F., Stevens, D. J., Russell, R. J., Gamblin, S. J., Skehel, J. J., and Kawaoka, Y. (2006) Haemagglutinin mutations responsible for the binding of H5N1 influenza A viruses to human-type receptors. *Nature 444*, 378–382.
13. Stevens, J., Blixt, O., Tumpey, T. M., Taubenberger, J. K., Paulson, J. C., and Wilson, I. A. (2006) Structure and receptor specificity of the hemagglutinin from an H5N1 influenza virus. *Science 312*, 404–410.
14. DeGrado, W. F., Summa, C. M., Pavone, V., Nastri, F., and Lombardi, A. (1999) De novo design and structural characterization of proteins and metalloproteins. *Annu. Rev. Biochem. 68*, 779–819.
15. Baltzer, L., and Nilsson, J. (2001) Emerging principles of de novo catalyst design. *Curr. Opin. Biotechnol. 12*, 355–360.
16. Bolon, D. N., Voigt, C. A., and Mayo, S. L. (2002) De novo design of biocatalysts. *Curr. Opin. Chem. Biol. 6*, 125–129.
17. Gibas, C., and Subramaniam, S. (1997) Knowledge-based design of a soluble bacteriorhodopsin. *Protein Eng. 10*, 1175–1190.
18. Hosse, R. J., Rothe, A., and Power, B. E. (2006) A new generation of protein display scaffolds for molecular recognition. *Protein Sci. 15*, 14–27.
19. Uchiyama, F., Tanaka, Y., Minari, Y., and Tokui, N. (2005) Designing scaffolds of peptides for phage display libraries. *J. Biosci. Bioeng. 99*, 448–456.
20. Rosinski, J. A., and Atchley, W. R. (1999) Molecular evolution of helix-turn-helix proteins. *J. Mol. Evol. 49*, 301–309.
21. Merritt, E. A., Sarfaty, S., van den Akker, F., L'Hoir, C., Martial, J. A., and Hol, W. G. (1994) Crystal structure of cholera toxin B-pentamer bound to receptor GM1 pentasaccharide. *Protein Sci. 3*, 166–175.
22. Kuziemko, G. M., Stroh, M., and Stevens, R. C. (1996) Cholera toxin binding affinity and specificity for gangliosides determined by surface plasmon resonance. *Biochemistry 35*, 6375–6784.
23. Harder, T., Scheiffele, P., Verkade, P., and Simons, K. (1998) Lipid domain structure of the plasma membrane revealed by patching of membrane components. *J. Cell Biol. 141*, 929–942.
24. Yanagisawa, K. (2007) Role of gangliosides in Alzheimer's disease. *Biochim. Biophys. Acta 1768*, 1943–1951.
25. Matsubara, T., Ishikawa, D., Taki, T., Okahata, Y., and Sato, T. (1999) Selection of ganglioside GM1-binding peptides by using a phage library. *FEBS Lett. 456*, 253–256.
26. Matsubara, T., Iijima, K., Nakamura, M., Taki, T., Okahata, Y., and Sato, T. (2007) Specific Binding of GM1-Binding Peptides to High-Density GM1 in Lipid Membranes. *Langmuir 23*, 708–714.
27. Fujitani, N., Shimizu, H., Matsubara, T., Ohta, T., Komata, Y., Miura, N., Sato, T., and Nishimura, S. (2007) Structural transition of a 15 amino acid residue peptide induced by GM1. *Carbohydr. Res. 342*, 1895–1903.
28. Gram, H., Marconi, L. A., Barbas, C. F., III, Collet, T. A., Lerner, R. A., and Kang, A. S. (1992) In vitro selection and affinity maturation of antibodies from a naive combinatorial immunoglobulin library. *Proc. Natl. Acad. Sci. U.S.A. 89*, 3576–3580.
29. Greenfield, N., and Fasman, G. D. (1969) Computed circular dichroism spectra for the evaluation of protein conformation. *Biochemistry 8*, 4108–4116.
30. Suzuki, N., and Fujii, I. (1999) Optimization of the loop length for folding of a helix loop helix peptide. *Tetrahedron Lett. 40*, 6013–6017.
31. Fujii, I., Takaoka, Y., Suzuki, K., and Tanaka, T. (2001) A conformationally purified α-helical peptide library. *Tetrahedron Lett. 42*, 3323–3325.
32. Rockendorf, N., Bade, S., Hirst, T. R., Gorris, H. H., and Frey, A. (2007) Synthesis of a fluorescent ganglioside G(M1) derivative and screening of a synthetic peptide library for G(M1) binding sequence motifs. *Bioconjugate Chem. 18*, 573–578.
33. Weis, W. I., and Drickamer, K. (1996) Structural basis of lectin-carbohydrate recognition. *Annu. Rev. Biochem. 65*, 441–473.
34. Hyun, S., Kim, J., Kwon, M., and Yu, J. (2007) Selection and syntheses of tentacle type peptides as 'artificial' lectins against various cell-surface carbohydrates. *Bioorg. Med. Chem. 15*, 511–517.
35. Yang, J. T., Wu, C.-S. C., and Martinez, H. M. (1986) Calculation of protein conformation from circular dichroism. *Methods Enzymol. 130*, 208–269.
36. Vila, J. A., Ripoll, D. R., and Scheraga, H. A. (2000) Physical reasons for the unusual α helix stabilization afforded by charged or neutral polar residues in alanine-rich peptides. *Proc. Natl. Acad. Sci. U.S.A. 97*, 13075–13079.
37. Gronow, S., and Brade, H. (2001) Lipopolysaccharide biosynthesis: Which steps do bacteria need to survive? *J. Endotoxin Res. 7*, 3–23.
38. Rudiger, H., and Gabius, H. J. (2001) Plant lectins: Occurrence, biochemistry, functions and applications. *Glycoconjugate J. 18*, 589–613.
39. Love, K. R., and Seeberger, P. H. (2002) Carbohydrate arrays as tools for glycomics. *Angew. Chem., Int. Ed. 41*, 3583–3586.
40. Hirabayashi, J., and Kasai, K. (2002) Separation technologies for glycomics. *J. Chromatogr., B 771*, 67–87.
41. Feizi, T., Fazio, F., Chai, W., and Wong, C. H. (2003) Carbohydrate microarrays: A new set of technologies at the frontiers of glycomics. *Curr. Opin. Struct. Biol. 13*, 637–645.
42. Matsubara, T., and Sato, T. (2007) Identification of oligosaccharide-recognition molecules by phage-display technology. *Trends Glycosci. Glycotechnol. 19*, 121–132.
43. Lis, H., and Sharon, N. (1998) Lectins: Carbohydrate-specific proteins that mediate cellular recognition. *Chem. Rev. 98*, 637–674.

BI8000837

Biochemical and Biophysical Research Communications 371 (2008) 230–235

Contents lists available at ScienceDirect

Biochemical and Biophysical Research Communications

journal homepage: www.elsevier.com/locate/ybbrc

Ganglioside GD1a suppresses TNFα expression via Pkn1 at the transcriptional level in mouse osteosarcoma-derived FBJ cells

Li Wang [a], Yinan Wang [a], Toshinori Sato [b], Sadako Yamagata [a], Tatsuya Yamagata [a,*]

[a] Laboratory of Tumor Biology and Glycobiology, Department of Life Sciences and Biopharmaceutics, Shenyang Pharmaceutical University, P.O. Box 29, 103 WenHua Road, Shenyang, LiaoNing 110016, People's Republic of China
[b] Department of Biosciences and Informatics, Keio University, Hiyoshi, Yokohama 223-8522, Japan

ARTICLE INFO

Article history:
Received 7 April 2008
Available online 22 April 2008

Keywords:
GD1a
TNFα
MMP-9
Cell motility
Pkn1
siRNA
Ganglioside

ABSTRACT

Ganglioside GD1a has been reported to suppress metastasis [S. Hyuga, S. Yamagata, Y. Takatsu, M. Hyuga, H. Nakanishi, K. Furukawa, T. Yamagata, Suppression of FBJ-LL cell adhesion to vitronectin by ganglioside GD1a and loss of metastatic capacity, International J. Cancer. 83 (1999) 685–691.] and MMP-9 production in mouse osteosarcoma FBJ cells [D. Hu, Z. Man, P. Wang, X. Tan, X. Wang, S. Takaku, S. Hyuga, T. Sato, X. Yao, S. Yamagata, T. Yamagata, Ganglioside GD1a negatively regulates MMP9 expression in mouse FBJ cell lines at the transcriptional level, Connect. Tissue Res. 48 (2007) 198–205.]. In the present study, TNFα increased cell motility and MMP-9 and TNFα expression at the transcriptional level. TNFα expression was found to be inversely proportional to GD1a content in the FBJ-cell variants. The addition of exogenous GD1a to FBJ-LL cells suppressed TNFα expression, and treatment of FBJ-S1 cells with D-PDMP (glucosylceramide synthesis inhibitor) led to an increase in TNFα, indicating that TNFα is negatively regulated by GD1a in FBJ cells. SiRNA of Pkn1, a Rho-GTPase effecter protein kinase, suppressed TNFα levels as well as Pkn1 expression, suggesting that Pkn1 is involved in TNFα signaling. Treatment of Pkn1-silenced FBJ-LL cells with GD1a failed to suppress TNFα expression, demonstrating that GD1a signals that lead to TNFα suppression are transduced through Pkn1.

Gangliosides, sialic acid-containing glycosphingolipids, have been demonstrated to have multifarious bioactivity in cells, including roles in immunoreaction and tumor progression [1,2]. The ganglioside GD1a has been demonstrated to regulate metastasis of osteosarcoma FBJ cells [3] possibly through enhancement of caveolin-1 and Stim1 [4] and suppression of MMP-9 [5]. GD1a and GT1b have been shown to induce the production of nitric oxide, tumor necrosis factor alpha (TNFα) and cyclooxygenase-2 in rat brain microglia [6]. GD1a blocks lipopolysaccharide-induced TNFα production and prevents maturation of human dendritic cells [7]. In monocytes, GD1a impairs antitumor immune responses by reducing the release of cytokines IL-6, IL-12, and TNFα [8]. The ganglioside GM3 has been shown to positively regulate TNFα production in mouse melanoma B16 cells with GM3 as the only ganglioside on the cell surface [9], through a PI3K, Rictor/mTOR, Akt, Arhgdib pathway [10].

Tumor necrosis factor alpha (TNFα) is a 17-kDa protein consisting of 157 amino acids, mainly produced by activated macrophages, T lymphocytes, and natural killer (NK) cells. It is a multifunctional cytokine involved in immune reactions, inflammation, cell apoptosis, and survival signals [11]. TNFα is known to work in an autocrine manner through two distinct receptors [12,13]. Secretion of MMP-9 can be enhanced in human vascular smooth muscle cells by stimulation of TNFα [14]. Rho family proteins are involved in TNFα-induced E-selectin and in the extravasation of tumor cells [15], along with TNFα-dependent adhesion of EC cells [16]. The protein kinase Pkn1, a down-stream effecter of Rho-GTPase, has been shown to contain Traf2-binding consensus sequences to activate the NFκB signal pathway [17].

In the present study, we have demonstrated that TNFα secreted by FBJ cells works in an autocrine manner, and is involved in elevated cell motility and MMP-9 secretion of FBJ cells. Expression of TNFα in FBJ cells was found to be negatively regulated by GD1a, and Pkn1 has been shown to be a key molecule in regulating TNFα expression and transducing GD1a signals, thereby leading to the suppression of TNFα in FBJ cells. To the best of our knowledge, this is the first study to show that Pkn1 is involved in ganglioside signals that regulate TNFα signaling and synthesis.

Materials and methods

Cell lines and culture. The highly metastatic mouse osteosarcoma cell line, FBJ-LL, and the poorly metastatic cell line, FBJ-S1, were produced from a FBJ virus-induced osteosarcoma of the BALB/c mouse [18]. LA5-30 cells were obtained by

* Corresponding author. Fax: +86 24 23986433.
E-mail address: tcyamagata@opal.dri.ne.jp (T. Yamagata).

0006-291X/$ - see front matter © 2008 Elsevier Inc. All rights reserved.
doi:10.1016/j.bbrc.2008.04.053

the transfection of FBJ-LL cells with GM2/GD2-synthase; mock-transfected M5 cells were the control [19]. The cells were maintained in RPMI-1640 media as described previously [4].

Chemicals and antibodies. Ganglioside GD1a and GM1 from bovine brain were purchased from Wako (Tokyo, Japan) and Toyobo (Osako, Japan), respectively. Recombinant TNFα was from Sigma (USA), and D-PDMP was from Matreya (USA). Rabbit anti-p-serine and rabbit anti-p-threonine antibodies were from ZYMED (USA) and CHEMICON (USA), respectively. Mouse anti-β-actin and hamster anti-TNFα antibodies were from Sigma (USA). Mouse anti-Pkn1 antibody was from BD (USA). HRP-linked anti-rabbit and anti-mouse secondary antibodies were from Cell Signaling (USA). POD-affinity anti-Syrian Hamster IgG secondary antibody was from Jackson (USA).

RNA extraction and RT-PCR. RNA extraction and analysis of amplified DNA have been described previously [4]. Primer sequences used for PCR in this study were as follows: for β-actin, sense 5′-ACACTGTGTGCCCATCTACGAGG-3′ and antisense 5′-AGGGGCCGGACTCGTCGTCATACT-3′; for MMP-9, sense 5′-CTGACTACGATAAG GACGGCAA-3′ and antisense 5′-ATACTGGATCCCGTCTATGTCG-3′; for TNFα, sense 5′-TCCAGGCGGTGCCTATGTCT-3′ and antisense 5′-GTTTGAGCTCAGCCCCCTCA-3′; for Pkn1, sense 5′-AGCCTTCAGCGCCATACTGC-3′ and antisense 5′-TGGTCTCGCCAGA ACACAGC-3′.

Construction of a TNFα expression vector. Total RNA was isolated from ascite macrophages of a Balb/c mouse using an RNeasy mini kit (Qiagen) according to the manufacturer's specifications. After first strand cDNA synthesis using TaKaRa RNA LA PCR Kit (AMV) (Takara Bio), a TNFα transcript was amplified using primers: sense, 5′-CAGGGATCCATGAGCACAGAAAGCATGATCCGCGAC-3′ and antisense, 5′-CAGGGATCCTCACAGAGCAATGACTCCAAAGTAGAC-3′. The PCR product was digested with BamHI and inserted into a pIRESpuro3 (Clonetech, USA) vector with puromycin resistance. Transient transfection to FBJ-LL cells was carried out with Fugene reagent (Roche, USA), essentially following the instructions of the manufacturer for mammalian cell transfection. Control cells received an empty vector. Puromycin resistant cells were screened as stable transfectants.

SiRNA and transfection. Selection of target sequences of Pkn1 siRNA was made using a Protein Lounge suggestion and Mulfold software. The target and scrambled sequence were 5′-GCAGGACAGTAAGACCAAGAT-3′ and 5′-TCGCGCTCCACATGATG ACTA-3′, respectively. The sequence was inserted into a retroviral vector with Neomycin resistance at TAKARA Biotechnology Corporation (China). Stable transfection was carried out as described previously [9].

Ganglioside extraction and HPTLC. Cells were grown to ~80% confluence in 10 cm dishes, harvested, and washed three times with PBS(−). Ganglioside extraction and HPTLC were performed as described previously [9].

Wound healing assay. For wound healing assays, monolayered confluent FBJ-LL cells were scraped manually with a pipette tip. Wound size was kept constant to ensure that all wounds had the same width. The cell culture media was replaced with serum-free media containing PBS(-) or TNFα (10 ng/ml). Wound closure was monitored by microscopy and microscopic pictures were taken of more than 10 different areas at 24 h, and number of cells that had moved into the vacant area was scored.

Transwell assay. FBS media (0.6 ml of 0.5%) were placed in the lower wells of a Transwell chamber (Costar, USA). FBJ-LL cells (1×10^5) in 0.1 ml of serum-free media containing PBS(−) or TNFα (10 ng/ml) were placed in each of the upper wells of the chamber. Cells were allowed to migrate for 24 h at 37 °C. Cells that translocated to the lower chamber were counted under the microscope (Nikon inverted TMD microscope, Japan).

Immunoprecipitation and Western blotting. FBJ-LL cells were harvested in a lysis buffer as described previously [4].

Gelatin zymography. FBJ cells were cultured in serum-free media for 12 h and aliquots of conditioned medium were subjected to gelatin zymography analysis, as described previously [20].

Statistical analysis. Data were analyzed using Microsoft Excel. All values are given as mean ± SD and levels of significance are indicated in figures. * indicates significance $P < 0.05$; **, significance $P < 0.01$; and ***, significance $P < 0.001$. NS, not significant.

Results

TNFα is involved in malignant property of FBJ cells and MMP-9 production

We have found that MMP-9 is critical for the migration capability of FBJ cells [20]. Because cytokine TNFα is reported to increase MMP-9 secretion in human vascular smooth muscle cells [14], we then asked if TNFα can affect the motility of FBJ cells. Treatment of FBJ-LL cells that have low levels of GD1a with TNFα (10 ng/ml) for 24 h increased cell motility by approximately 2-fold as judged by wound healing (Fig. 1A) and Transwell experiments (Fig. 1B), implying that TNFα is an important molecule in the malignant properties of FBJ cells.

In order to know whether stimulated motility is related to MMP-9 expression, we cultured several lines of cells in the presence of TNFα (10 ng/ml) for 12 h. The cell lines used in this experiment were: highly metastatic FBJ-LL cells; poorly metastatic FBJ-S1 cells [21]; FBJ-5-30 cells, transfectants that GD1a to the same level as FBJ-S1 cells; and FBJ-M5 cells, the vector control from when FBJ-LL was transfected with GM2/GD2-synthase cDNA [19]. The addition of TNFα to the culture media of any cell line resulted in elevated mRNA synthesis of both MMP-9 (Fig. 1C) and TNFα (Fig. 1D), indicating that MMP-9 and TNFα expression was stimulated by TNFα at the transcriptional level. Aliquots of culture media were subjected to gelatin zymography and the intensity of MMP-9 bands was enhanced by TNFα treatment in each of FBJ cell lines (Fig. 1E). There was no sign of MMP-2 expression in cells treated with TNFα (data not shown).

The induction of MMP-9 by TNFα was further confirmed by transfection of TNFα cDNA into FBJ-LL cells. TNFα levels in stable transfectants were about three times higher than in mock-cDNA-transfected cells. MMP-9 production was also enhanced 3-fold (Fig. 1F). Cell motility of TNFα-transfected cells was highly activated as compared to mock-transfected cells (data not shown), confirming the above results. Taken together, these results clearly demonstrate that TNFα is secreted in an autocrine manner and that TNFα produced in the manner is sure to be involved in elevated cell motility and the production of TNFα and MMP-9.

TNFα is negatively regulated by GD1a in FBJ cells

GD1a has been demonstrated to regulate the metastasis of mouse FBJ-virus-induced osteosarcoma cells [19], possibly through suppression of MMP-9 [5], and in this study, TNFα has been shown to increase MMP-9 secretion. As a result, we were curious about possible regulation of TNFα by GD1a. As revealed by RT-PCR, TNFα expression in FBJ-LL cells was four times higher than in FBJ-S1 cells. This was also the case for FBJ-M5 cells as compared to FBJ-5-30 cells (Fig. 2A and B). Evaluation of TNFα at the protein level (assayed in LL and S1 cells by Western blot) showed that protein levels follow the same patterns as mRNA levels (Fig. 2C and D). GD1a content in FBJ-LL, -S1, M5, and LA5-30 cells (Fig. 2A) shows an inverse relationship between TNFα expression and GD1a content, and suggests that GD1a negatively regulates TNFα in FBJ cells.

Exogenous addition of GD1a (50 μM) to FBJ-LL and FBJ-M5 cells decreased TNFα mRNA levels to a half that of control cells at 12 h (Fig. 3A). Treatment of FBJ-S1 and FBJ-LA5-30 cells with 12.5 μM D-PDMP (an inhibitor of glucosylceramide synthesis) for six days resulted in increased TNFα expression (Fig. 3B) as well as depletion of gangliosides (Fig. 3C). These results clearly support the idea that GD1a negatively regulates TNFα production in FBJ cells. When FBJ-M5 cells were treated with GM1 (50 μM), we found that, besides GD1a, GM1 also decreased TNFα expression (Fig. 3D). In FBJ cells, TNFα augmented TNFα and MMP-9 levels (Fig. 1C and D) that were suppressed in the presence of 50 μM GD1a (Fig. 3E), suggesting that autocrine Tnfα effects are suppressed by GD1a. Taken together, the above results strongly indicate that TNFα expression is negatively regulated by GD1a in FBJ cells.

GD1a down-regulates TNFα expression via Pkn1

In order to identify molecules involved in GD1a signaling during the regulation of TNFα, a protein phosphorylation profile analysis was performed by Kinexus Co. (USA). Among the proteins with altered phosphorylation, a Rho-GTPase associated protein kinases Pkn1 and Pkn2 along with Pdpk1 had enhanced phosphorylation in FBJ-5-30 cells as compared with FBJ-M5 cells (Supplementary Fig. S1). Phosphorylation was measured at serine and threonine residues of Pkn1 isolated from FBJ-LL cells that had been stimu-

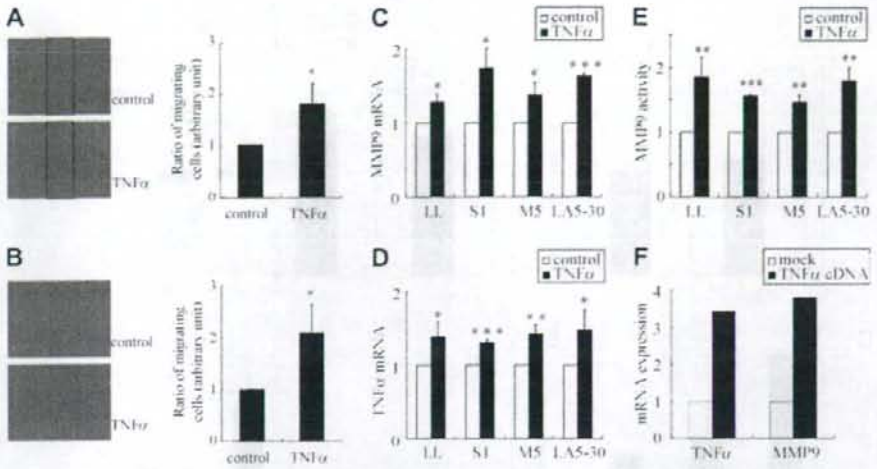

Fig. 1. TNFα stimulated motility of FBJ-LL cells and MMP-9 and TNFα production at the transcriptional level. (A) Wound healing assay of FBJ-LL cells in serum-free RPMI-1640 containing PBS (−) or TNFα (10 ng/ml). (B) Transwell translocation assay using FBJ-LL cells in serum-free media containing PBS (−) or TNFα (10 ng/ml). FBJ cells were treated with TNFα (10 ng/ml) in serum-free media for 12 h, and then total RNA was extracted and subjected to RT-PCR. The amount of MMP-9 or TNFα thus amplified was normalized to β-actin (as a housekeeping gene) and the expression of MMP-9 (C) or TNFα (D) of TNFα treated cells was expressed as the ratio to the control. Conditioned media of FBJ cells that had been incubated in serum-free media with or without TNFα (10 ng/ml) for 12 h was collected and subjected to gelatin zymography (E). FBJ-LL cells were transfected with a TNFα cDNA or with an empty vector (mock), and the expression of TNFα and MMP-9 was determined by RT-PCR (F). The pictures are representative and the data from (A) to (E) are the means of three independent experiments.

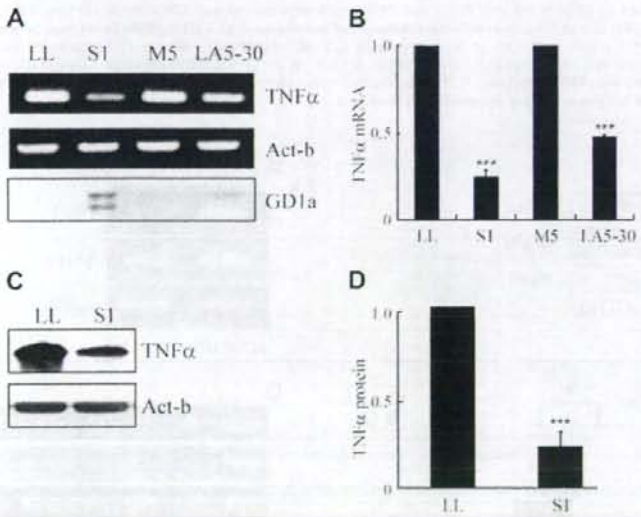

Fig. 2. Inverse relationship of TNFα expression to GD1a content in FBJ cells. mRNA expression of TNFα compared with β-actin in FBJ cells as determined by RT-PCR (A). The bottom panel in (A) represents GD1a content in FBJ cells as revealed by HPTLC. In (B), TNFα expression (normalized to β-actin) in FBJ cells is shown; expression in FBJ-LL cells is set at 1. Cell lysates of FBJ-LL and FBJ-S1 cells were subjected to Western blots to determine expression of TNFα protein levels, with β-actin as an internal control (C). Visualization of panel (C) is given in (D), where TNFα expression in FBJ-LL cells is set at 1. Pictures are representative and the data are the means of three independent experiments.

lated with 50 μM GD1a for 15 min, followed by immunoprecipitation with an anti-Pkn1 antibody. Fig. 4A shows that phosphorylation at serine and threonine residues was enhanced by GD1a stimulation of cells, suggesting that Pkn1 plays a role in GD1a signaling related to TNFα production.

In order to prove that Pkn1 is involved in GD1a signal transduction resulting in suppression of TNFα, polyclonal and monoclonal stable Pkn1 siRNA-transfected cells were obtained; Pkn1 expression was successfully impaired in these cell lines. TNFα expression was suppressed in Pkn1-silenced polyclonal cells (Fig. 4B) and in Pkn1-silenced monoclonal cells (Fig. 4D), suggesting the involvement of Pkn1 in TNFα signaling. The addition of GD1a (50 μM) to the scrambled siRNA-transfected LL cells decreased TNFα expression to similar levels as FBJ-LL cells, while treatment of

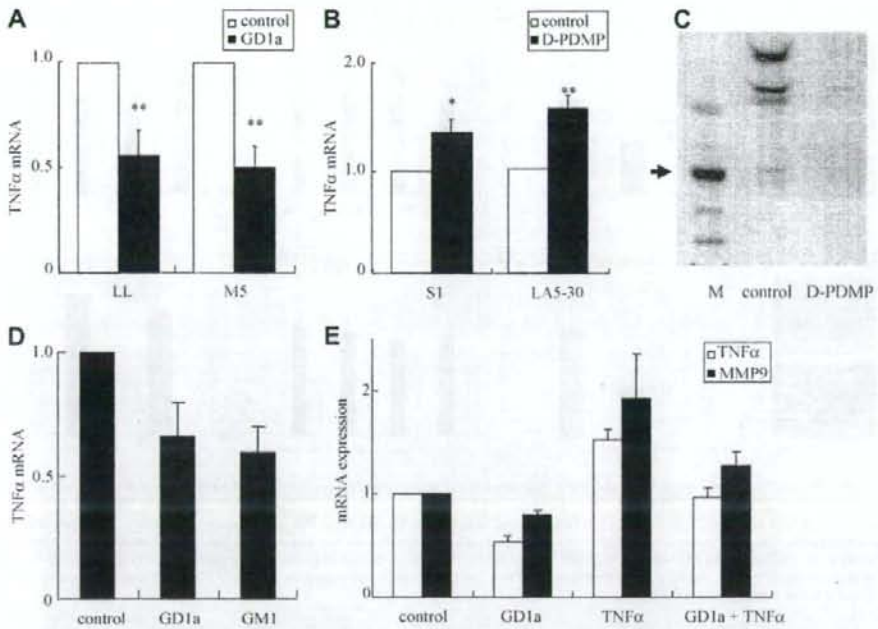

Fig. 3. TNFα was negatively regulated by GD1a in FBJ cells. FBJ-LL and FBJ-M5 cells were treated with GD1a (50 μM) in serum-free media for 12 h, then total RNA was extracted and subject to RT-PCR (A). FBJ-S1 and FBJ-LA5-30 cells were cultured in the presence of 12.5 μM D-PDMP for six days in complete media that was changed every day, then subject to RT-PCR (B). HPTLC pattern of FBJ-LA5-30 cells treated with 12.5 μM D-PDMP for six days in (C). M stands for brain ganglioside mixture, and an arrow shows the position of GD1a. (D), FBJ-M5 cells were treated with GD1a (50 μM) or GM1 (50 μM) in serum-free media for 12 h, and the expression of TNFα was determined by RT-PCR. (E) FBJ-LL cells were treated with TNFα (10 ng/ml), GD1a (50 μM), and TNFα (10 ng/ml) plus GD1a (50 μM) for 12 h, and expression of TNFα and MMP-9 was determined by RT-PCR. The data are the means of three independent experiments.

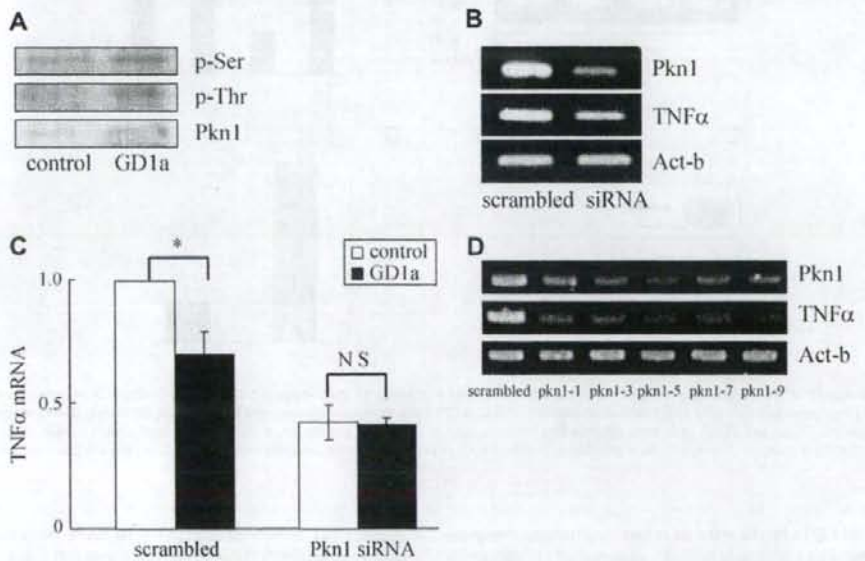

Fig. 4. GD1a suppresses TNFα through Pkn1. Phosphorylation of serine and threonine residues of Pkn1 in FBJ-LL cells that had been stimulated with GD1a (50 μM) for 15 min without serum was determined by immunoprecipitation with Pkn1 antibody, followed by SDS–PAGE and Western blot with the individual phospho-specific antibodies (A). FBJ-LL cells were transfected with either Pkn1 siRNA or scrambled sequence siRNA, followed by selection with G418. Pkn1 and TNFα mRNA expression was determined by RT-PCR with β-actin as a control in polyclonal (B) or in individual monoclonal cells (D). In (C), Pkn1 siRNA or scrambled siRNA-transfected polyclonal cells were incubated with 50 μM GD1a, and TNFα expression was determined by RT-PCR with β-actin as a control. Results are shown with TNFα mRNA of the control cells set to 1. The pictures are representative and the data in (C) are the means of three independent experiments.

Pkn1-silenced polyclonal cells with GD1a failed to reduce TNFα expression (Fig. 4C), distinctly supporting the notion that GD1a signals are transduced to TNFα through Pkn1.

Discussion

GD1a enhances the FBJ-cell expression of caveolin-1 and Stim1 [4], which are known tumor suppressor genes. GD1a suppresses cell motility [3], adhesion to vitronectin [19], and MMP-9 production in FBJ cells [5,20]. In the present study, we have provided evidence that in FBJ cells, TNFα is under the negative control of GD1a via Pkn1. Besides GD1a, ganglioside GM1 also suppressed TNFα expression in M5 cells, indicating that suppression of TNFα by GD1a was not specific to GD1a. The amount of GM1 present in FBJ cells is scant, and its contribution to cell activity may be negligible. SiRNA targeting GD1a-synthase St3gal2 suppressed GD1a production significantly, but did not increase expression of TNFα (data not shown). Since GM1 was as effective as GD1a at decreasing TNFα expression, it is plausible that in the St3gal2 siRNA-transfected cells, GM1 accumulates and functions in place of GD1a. Ganglioside GM3 cannot affect TNFα expression in FBJ cells (data not shown), though GM3 has been reported to positively regulate TNFα at the level of transcription in melanoma B16 cells [9] through the Arhgdib pathway [10]. GD3 was reported to inhibit TNFα induction of MMP-9 via inhibition of p-ERK in human vascular smooth muscle cells [22]. Several lines of evidence imply that the mechanism of regulation of TNFα by gangliosides is not the same in different cell types.

TNFα binds to two different receptors, Tnfrsf1a and Tnfrsf1b [13]. The essential difference between the receptors lies in the death domain of Tnfrsf1a that is absent in Tnfrsf1b. For this reason, Tnfrsf1a can induce apoptosis by recruiting death domain-containing adaptor proteins and activate caspase 8 [23]. In the present study, we have shown that TNFα enhanced FBJ cells motility and cells did not undergo apoptosis (data not shown). It is not clear which TNFα receptors are involved in TNFα signaling in FBJ cells. Research on the mechanism of action of TNFα in FBJ cells is under way in our laboratory.

Since a Kinexus analysis showed that Pkn1 phosphorylation of GD1a-rich FBJ-5-30 cells was activated 3.3 times as high at Thr778 (comparable to Thr774 in human) as GD1a-deficient FBJ-M5 cells (Supplementary Fig. S1), that phosphorylation at Thr774 by Pdpk1 results in Pkn1 activation [24], and we verified that phosphorylation at Thr residues of Pkn1 was high in FBJ-S1 cells than FBJ-LL cells (data not shown), we hypothesized that phosphorylation of Pkn1 in FBJ-LL cells could be activated by GD1a treatment. Phosphorylation at Thr and Ser residues was increased upon GD1a treatment of FBJ-LL cells (Fig. 4). This does not necessarily prove that Pkn1 at Thr778 was phosphorylated by the GD1a signals, but this result is consistent with the analysis of Kinexus and may imply that the GD1a signals have stimulated Pkn1. Pkn1 participation in GD1a signaling will be unambiguously shown if Pkn1 silencing may block the GD1a signals leading to TNFα suppression. Thus, we transfected Pkn1 siRNA into FBJ-LL cells and demonstrated the successful impairment of Pkn1 expression. Pkn1 silencing in FBJ-LL cells significantly lowered TNFα expression, and treatment of these cells with GD1a did not further reduce TNFα expression, whereas treatment of control cells with GD1a notably decreased TNF expression. This result supports the notion that the GD1a signals that lead to TNF suppression go through Pkn1. This is the first paper describing the involvement of Pkn1 in TNF production, and that the GD1a signal is transduced via the Pkn1 pathway. Research to elucidate molecular events up-stream and down-stream of Pkn1 in GD1a-regulated TNFα signals is currently on-going in our laboratory.

Acknowledgment

This work was in part supported by a fund from Mizutani Foundation for Glycoscience (to T.Y.).

Appendix A. Supplementary data

Ganglioside GD1a suppresses TNFα expression via Pkn1 at the transcriptional level in mouse osteosarcoma-derived FBJ cells. Supplementary data associated with this article can be found, in the online version, at doi:10.1016/j.bbrc.2008.04.053.

References

[1] D.M. Marcus, A review of the immunogenic and immunomodulatory properties of glycosphingolipids, Mol. Immunol. 21 (1984) 1083–1091.
[2] S. Hakomori, Tumor malignancy defined by aberrant glycosylation and sphingo (glyco) lipid metabolism, Cancer Res. 56 (1996) 5309–5318.
[3] S. Hyuga, S. Yamagata, T. Tai, T. Yamagata, Inhibition of highly metastatic FBJ-LL cell migration by ganglioside GD1a highly expressed in poorly metastatic FBJ-S1 cells, Biochem. Biophys. Res. Commun. 231 (1997) 340–343.
[4] L. Wang, S. Takaku, P. Wang, D. Hu, S. Hyuga, T. Sato, S. Yamagata, T. Yamagata, Ganglioside GD1a regulation of caveolin-1 and Stim1 expression in mouse FBJ cells: augmented expression of caveolin-1 and Stim1 in cells with increased GD1a content, Glycoconj. J. 23 (2006) 303–315.
[5] D. Hu, Z. Man, P. Wang, X. Tan, X. Wang, S. Takaku, S. Hyuga, T. Sato, X. Yao, S. Yamagata, T. Yamagata, Ganglioside GD1a negatively regulates MMP9 expression in mouse FBJ cell lines at the transcriptional level, Connect. Tissue Res. 48 (2007) 198–205.
[6] H. Pyo, E. Joe, S. Jung, S.H. Lee, I. Jou, Gangliosides activate cultured rat brain microglia, J. Biol. Chem. 274 (1999) 34584–34589.
[7] W. Shen, S. Ladisch, Ganglioside GD1a impedes lipopolysaccharide-induced maturation of human dendritic cells, Cell. Immunol. 220 (2002) 125–133.
[8] S. Caldwell, A. Heitger, W. Shen, Y. Liu, B. Taylor, S. Ladisch, Mechanisms of ganglioside inhibition of APC function, J. Immunol. 171 (2003) 1676–1683.
[9] P. Wang, P. Wu, J. Zhang, T. Sato, S. Yamagata, T. Yamagata, Positive regulation of tumor necrosis factor alpha by ganglioside GM3 through Akt in mouse melanoma B16 cells, Biochem. Biophys. Res. Commun. 356 (2007) 438–443.
[10] P. Wang, X. Yang, P. Wu, J. Zhang, T. Sato, S. Yamagata, T. Yamagata, GM3 signals regulating Tnf-alpha expression are mediated by Rictor and Arhgdib in mouse melanoma B16 cells, Oncology (in press).
[11] R.M. Locksley, N. Killeen, M.J. Lenardo, The TNF and TNF receptor superfamilies: integrating mammalian biology, Cell 104 (2001) 487–501.
[12] J.T. Schroeder, K.L. Chichester, A.P. Bieneman, Toll-like receptor 9 suppression in plasmacytoid dendritic cells after IgE-dependent activation is mediated by autocrine TNF-alpha, J. Allergy Clin. Immunol. 121 (2008) 486–491.
[13] S. Gupta, A decision between life and death during TNFα-induced signaling, J. Clin. Immunol. 22 (2002) 185–194.
[14] S.K. Moon, B.Y. Cha, C.H. Kim, ERK1/2 mediates TNF-alpha induced matrix metalloproteinase-9 expression in human vascular smooth muscle cells via the regulation of NF-kappaB and AP-1: involvement of the Ras dependent pathway, J. Cell. Physiol. 198 (2004) 417–427.
[15] T. Nübel, W. Dippold, H. Kleinert, B. Kaina, G. Fritz, Lovastatin inhibits Rho-regulated expression of E-selectin by TNFalpha and attenuates tumor cell adhesion, FASEB J. 18 (2004) 140–142.
[16] X.L. Chen, Q. Zhang, R. Zhao, X. Ding, P.E. Tummala, R.M. Medford, Rac1 and superoxide are required for the expression of cell adhesion molecules induced by tumor necrosis factor-alpha in endothelial cells, J. Pharmacol. Exp. Ther. 305 (2003) 573–580.
[17] Y. Gotoh, K. Oishi, H. Shibata, A. Yamagiwa, T. Isagawa, T. Nishimura, E. Goyama, M. Takahashi, H. Mukai, Y. Ono, Protein kinase PKN1 associates with TRAF2 and is involved in TRAF2-NF-kappaB signaling pathway, Biochem. Biophys. Res. Commun. 314 (2004) 688–694.
[18] S. Yamagata, M. Miwa, K. Tanaka, T. Yamagata, FBJ virus-induced osteosarcoma has type V collagen consisting of A, B and C-like chains in addition to type I collagen, Biochem. Biophys. Res. Commun. 105 (1982) 1208–1214.
[19] S. Hyuga, S. Yamagata, Y. Takatsu, M. Hyuga, H. Nakanishi, K. Furukawa, T. Yamagata, Suppression of FBJ-LL cell adhesion to vitronectin by ganglioside GD1a and loss of metastatic capacity, Int. J. Cancer 83 (1999) 685–691.
[20] D. Hu, X. Tan, T. Sato, S. Yamagata, T. Yamagata, Apparent suppression of MMP-9 activity by GD1a as determined by gelatin zymography, Biochem. Biophys. Res. Commun. 349 (2006) 426–431.

[21] S. Yamagata, Y. Ito, R. Tanaka, S. Shimizu, Gelatinase of metastatic cell lines of murine colonic carcinoma as detected by substrate-gel electrophoresis, Biochem. Biophys. Res. Commun. 151 (1988) 158–162.
[22] S.K. Moon, S.K. Kang, C.H. Kim, Reactive oxygen species mediates disialoganglioside GD3-induced inhibition of ERK1/2 and matrix metalloproteinase-9 expression in vascular smooth muscle cells, FASEB J. 20 (2006) 1387–1395.
[23] J. Zhou, M. Zhang, S.S. Atherton, Tumor necrosis factor-alpha-induced apoptosis in murine cytomegalovirus retinitis, Invest. Ophthalmol. Vis. Sci. 48 (2007) 1691–1700.
[24] L.Q. Dong, L.R. Landa, M.J. Wick, L. Zhu, H. Mukai, Y. Ono, F. Liu, Phosphorylation of protein kinase N by phosphoinositide-dependent protein kinase-1 mediates insulin signals to the actin cytoskeleton, Proc. Natl. Acad. Sci. USA 97 (2000) 5089–5094.

Biochimica et Biophysica Acta 1778 (2008) 2717–2726

Contents lists available at ScienceDirect

Biochimica et Biophysica Acta

journal homepage: www.elsevier.com/locate/bbamem

Age-dependent high-density clustering of GM1 ganglioside at presynaptic neuritic terminals promotes amyloid β-protein fibrillogenesis

Naoki Yamamoto [a,b,1], Teruhiko Matsubara [c], Toshinori Sato [c], Katsuhiko Yanagisawa [a,*]

[a] Department of Alzheimer's Disease Research, National Institute for Longevity Sciences, National Center for Geriatrics and Gerontology, Obu 474-8522, Japan
[b] Japan Society for the Promotion of Sciences (JSPS), Tokyo 102-8472, Japan
[c] Department of Biosciences and Informatics, Keio University, Yokohama 223-8522, Japan

ARTICLE INFO

Article history:
Received 15 May 2008
Received in revised form 15 July 2008
Accepted 30 July 2008
Available online 7 August 2008

Keywords:
Alzheimer's disease
Amyloid β-protein
GM1 ganglioside
Aging
Synapse

ABSTRACT

The deposition of amyloid β-protein (Aβ) is an invariable feature of Alzheimer's disease (AD); however, the biological mechanism underlying Aβ assembly into fibrils in the brain remains unclear. Here, we show that a high-density cluster of GM1 ganglioside (GM1), which was detected by the specific binding of a novel peptide (p3), appeared selectively on synaptosomes prepared from aged mouse brains. Notably, the synaptosomes bearing the high-density GM1 cluster showed extraordinary potency to induce Aβ assembly, which was suppressed by an antibody specific to GM1-bound Aβ, an endogenous seed for AD amyloid. Together with evidence that Aβ deposition starts at presynaptic terminals in the AD brain and that GM1 levels significantly increase in amyloid-positive synaptosomes prepared from the AD brain, our results suggest that the age-dependent high-density GM1 clustering at presynaptic neuritic terminals is a critical step for Aβ deposition in AD.

1. Introduction

Evidence is accumulating that the interaction of amyloid β-protein (Aβ) with lipid membranes is an early event in its fibril formation in Alzheimer's disease (AD) [1–3]. Previous *in vitro* studies suggested that particular lipid constituents such as cholesterol can be a binding partner for Aβ [4–6]. However, the nature of neuronal membranes responsible for inducing Aβ assembly remains to be determined. We previously identified GM1-ganglioside (GM1)-bound Aβ (GAβ) in the brain that showed early pathological changes associated with AD [7,8]. To date, a number of *in vitro* and *in vivo* studies regarding GAβ have supported the possibility that GAβ acts as an endogenous seed for amyloid fibril formation in the AD brain [9–17]. Yet despite the lines of evidence in favor of this possibility, the GAβ hypothesis has been challenged by a simple question concerning how GAβ is generated in the AD brain.

To explore the mechanism underlying GAβ generation in the brain, we previously examined the lipid composition of synaptosomes prepared from mouse brains at different ages [18]. The prominent findings in that study were as follows. First, the GM1 levels in detergent-resistant membrane microdomains (DRMs) prepared from synaptosomes significantly increased with age and the increase was markedly pronounced in synaptosomes from the human apolipoprotein E4 (apoE4)-knock-in mouse brains compared with those from the apoE3-knock-in mouse brains. Second, the DRMs possessed unique biochemical features distinct from those of lipid rafts; for example, the GM1 accumulation in the DRMs was resistant to methyl-β-cyclodextrin (MβCD) treatment, which is frequently used to destroy cholesterol- and GM1-rich membrane microdomains such as lipid rafts [19,20]. Third, Aβ assembly to amyloid fibril formation was markedly accelerated in the presence of the synaptosomes bearing the DRMs. Together with a previous finding that Aβ deposition likely starts at presynaptic terminals in AD brains [21,22], these findings imply the pathological significance of GM1 accumulation at presynaptic neuritic terminals in AD. Furthermore, this possibility has been supported by a recent study showing that the GM1 levels significantly increase in the amyloid-positive synaptosomes compared with amyloid-free synaptosomes prepared from AD brains [23].

The purpose of this study was to clarify the nature of the GM1-rich, MβCD-resistant DRMs (GMD). Here, we describe that GMD, with a high potency to induce Aβ fibril formation, selectively appeared in synaptosomes but not in non-synaptosomes prepared from mouse brains. Importantly, the synaptosomes bearing the GMD were characterized by their high-density GM1 clustering, which was specifically recognized using a novel peptide (p3; VWRLLAPPFSNRLLP) [24]. Notably, the high-density GM1 clustering in synaptosomes was an age-dependent, and partially, brain-region-specific event. Finally, it was also suggested that sphingomyelin (SM) plays a role in inducing the high-density GM1 clustering in presynaptic plasma membranes.

* Corresponding author. Department of Alzheimer's Disease Research, National Institute for Longevity Sciences, National Center for Geriatrics and Gerontology, 36-3 Gengo, Morioka, Obu 474-8522, Japan. Tel.: +81 562 44 5651x5002; fax: +81 562 44 6594.
E-mail address: katuhiko@nils.go.jp (K. Yanagisawa).
[1] Present affiliation and address: Department of Pharmacy, College of Pharmaceutical Sciences, Ritsumeikan University, Kusatsu 525-8577, Japan.

0005-2736/$ – see front matter © 2008 Elsevier B.V. All rights reserved.
doi:10.1016/j.bbamem.2008.07.028

2. Materials and methods

2.1. Preparation of synaptosomes and non-synaptosomes

Synaptosomes were prepared as previously described [25,26]. A hippocampus or a whole brain minus the hippocampus, cerebellum and brainstem, was homogenized in 0.32 M sucrose buffer containing 0.25 mM EDTA. The homogenate was centrifuged at 580 ×g for 8 min. The supernatant (post-nuclear supernatant) was centrifuged at 14,500 ×g for 20 min. The resulting pellet (crude mitochondrial pellet) was suspended in 0.32 M sucrose buffer without EDTA, layered over Ficoll in sucrose buffer, and then, centrifuged at 87,000 ×g for 30 min. The resultant interface was collected as the source of synaptosomes. On the other hand, the supernatant obtained by the centrifugation of the post-nuclear supernatant was combined with the upper phase obtained by the centrifugation of the suspension of the crude mitochondrial pellet, and then, further centrifuged at 540,000 ×g for 30 min. The resultant pellet was collected as the source of non-synaptosomes.

2.2. Electron microscopy

The synaptosomes isolated from brain homogenates were diluted and then spread on carbon-coated grids, allowing each solution to stand for 2 min before removing excess solution using a filter paper. After drying, the grids were negatively stained with 2% uranyl acetate. Micrographs were obtained by transmission electron microscopy using a JEM-2000EX (JEOL, Tokyo, Japan) with an acceleration voltage of 100 kV.

2.3. Isolation of DRMs

The DRMs were prepared from the synaptosomes and non-synaptosomes according to a previously established method [18]. Briefly, synaptosomes (0.2 mg protein/ml) were homogenized in MES-buffer saline (MBS) containing 1% Triton X-100. The sucrose concentration of the extract was adjusted to 40% by the addition of 80% sucrose in MBS, and then they were overlaid with a 5%/35% discontinuous sucrose gradient in MBS without Triton X-100, followed by centrifugation at 188,000 ×g for 20 h using an SW41-Ti rotor (Beckman, Palo Alto, CA). After centrifugation, 1-ml fractions were harvested from the top to the bottom of the gradient. Success of DRM isolation was verified by confirmation of GM1 enrichment in the fifth fraction as had been reported in our previous study [18].

2.4. SDS-PAGE and Western blotting

The protein concentration of each sample was determined using a BCA protein assay kit (Pierce, Rockford, IL) with bovine serum albumin (BSA) as the standard. The samples were separated by sodium dodecyl sulfate-polyacrylamide gel electrophoresis (SDS-PAGE) and then electrotransferred onto NitroBind membrane (GE Osmonics, Minnetonka, MN). The blots were probed with, monoclonal antibodies specific to SNAP25, syntaxin, nucleaporin p62, aquaporin 4 (AQP4) or CTB-HRP, which were purchased from Stressgen (Victoria, Canada), Santa Cruz (CA, USA), BD Bioscience Pharmingen (CA, USA) Millipore (MA, USA) and SIGMA-Aldrich (MO, USA), respectively. The bands were visualized using an ECL detection system (GE Healthcare, Piscataway, NJ).

2.5. Levels of sphingomyelin, GM1, phospholipids and cholesterol

The sphingomyelin levels in the samples were determined by TLC and scanning densitometry. Lipids were extracted using chloroform/methanol/water 52:26:21 by volume. The lower phase was removed, and the solvent was evaporated and solubilized in chloroform/methanol 70:30 by volume. The lipid extract was spotted onto high-performance TLC plates (Merck, Darmstadt, Germany) and run in three separate solvent systems: methyl acetate/1-propanol/chloroform/methanol/0.25% KCl solution 25:25:25:10:9 by volume; *n*-hexane/diethyl ether/acetic acid 75:23:2 by volume; and *n*-hexane. After each run, the plate was thoroughly dried using hot air. Lipid spots were visualized by dipping the plates in a mixture of 10% $CuSO_4 \cdot 5H_2O$, 8% H_3PO_4, then placing them vertically on paper towels for 1 min to drain the excess charring reagent, followed by heating for 10–20 min at 170 °C. Quantification was performed using NIH image version 1.59 software. The GM1 level in the samples was determined by blot analysis using cholera toxin B subunit-horseradish peroxidase conjugated (CTX-HRP) as previously reported [7]. The cholesterol and phospholipid levels in the samples were determined using Determiner L (Kyowa, Tokyo, Japan) and Phospholipids C (Wako, Osaka, Japan), respectively.

2.6. Aβ incubation in the presence of synaptosomes

Seed-free solutions of Aβ (Aβ1–40) (Peptide Inst., Osaka, Japan) were prepared as previously described [27]. Aβ solutions at 50 μM in Tris-buffered saline (TBS1: 10 mM Tris–HCl and 150 mM NaCl, pH 7.4) were incubated at 37 °C with or without synaptosomes. The fluorescence intensities of Thioflavin T (ThT), which specifically recognizes the amyloid structure, of the mixture incubated for 24 h were determined as previously described [15].

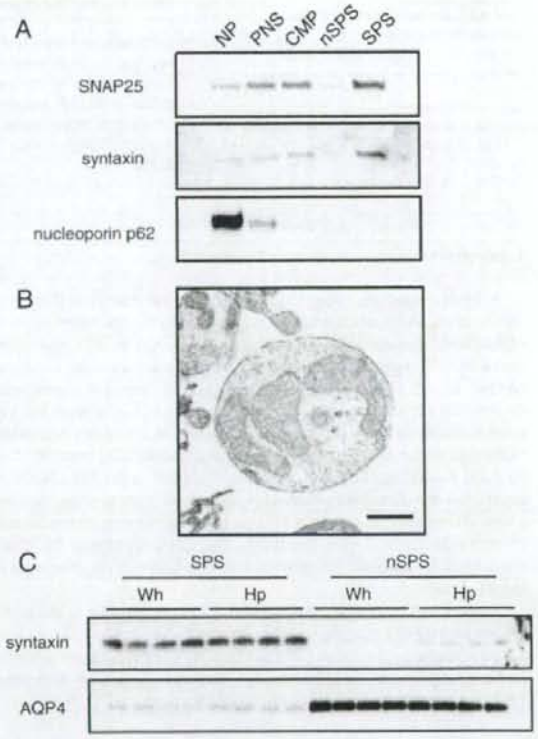

Fig. 1. Characterization of the synaptosomal and non-synaptosomal fractions. (A) Fractions obtained from the preparation of the synaptosomal and non-synaptosomal fractions were subjected to Western blot analysis using monoclonal antibodies specific to SNAP25, syntaxin and nucleoporin p62. (B) The prepared synaptosomes were negatively stained and examined by electron microscopy. Scale bar: 500 nm. (C) The synaptosomal and non-synaptosomal fractions obtained from four animals were subjected to Western blotting assay using monoclonal antibodies specific to syntaxin and AQP4. NP; nuclear pellet, PNS; post-nuclear supernatant, CMP; crude mitochondrial pellet, nSPS; non-synaptosomal fraction, SPS; synaptosomal fraction, Wh: whole brain minus the hippocampus, cerebellum and brainstem, Hp: hippocampus.

2.7. Methyl-β-cyclodextrin (MβCD) treatment

The synaptosomes were washed with Tris-buffered saline (TBS2; 20 mM Tris–HCl, 150 mM NaCl, pH 7.4) at 4 °C and then resuspended in TBS2 with or without 10 mM MβCD. After incubation at 37 °C for 30 min, the mixture was centrifuged at 17,000 ×g for 15 min. The resultant precipitates were subjected to assay or fractionation for DRMs.

2.8. Fluorescence staining of GM1 clustering

Synaptosomes and non-synaptosomes were seeded on poly-L-lysine-coated 24-well plates at a total protein content of 3 μg and incubated either with or without biotin-conjugated p3 (VWRLLAP PFSNRLLP, 300 nM) at room temperature for 1 h. After washing with PBS, the synaptosomes were incubated with Alexa Fluor 594-conjugated streptavidin (10 μg/ml) for 1 h. The synaptosomes incubated alone with Alexa Fluor 594-conjugated streptavidin without p3 treatment did not show labeling.

2.9. Inhibition of membrane-bound neutral sphingomyelinase

PC12 cells were cultured in Dulbecco's modified Eagle's medium (DMEM, Invitrogen, Carlsbad, CA) supplemented with 10% heat-inactivated horse serum and 5% FBS. For their differentiation, PC12 cells were plated on poly-L-lysine-coated (10 mg/ml) chamber slides (Nunc, Roskilde, Denmark) at a density of 50,000 cells/cm^2 and cultured for 6 days in DMEM supplemented with 100 ng/ml nerve growth factor (NGF; Alomone Labs, Jerusalem, Israel). The cells were treated with GW4869 (Calbiochem, Darmstadt, Germany). After 2 days, the cells were fixed with 4% formaldehyde and incubated with 5% BSA blocking agent. The cells were then incubated with biotin-conjugated p3 and Alexa Fluor 488-coupled CTX at room temperature for 1 h. After washing with PBS, the cells were incubated with Alexa Fluor 594-conjugated streptavidin (10 μg/ml) for 1 h.

3. Results

3.1. Characterization of synaptosomes and non-synaptosomes

The isolated synaptosomes were characterized by Western blot analysis using monoclonal antibodies specific to SNAP-25 and syntaxin, which are abundant in presynaptic plasma membrane, and nucleoporin p62, which exclusively localizes at the nuclear membrane [28]. As shown in Fig. 1A, the presynaptic marker proteins were abundant in the synaptosome fractions whereas the nuclear protein was absent in these fractions. Moreover, electron microscopy of the synaptosome fractions revealed typical structural characteristics of synaptosomes with the presence of recognizable mitochondria (Fig. 1B). To compare the characteristics of the isolated synaptosomes and non-synaptosomes, we performed Western blot analysis using monoclonal antibodies specific to syntaxin and AQP4, which is exclusively abundant in astrocyte plasma membrane [29]. As shown in Fig. 1C, the presence of syntaxin and AQP4 in the synaptosomes and non-synaptosomes were mutually exclusive.

3.2. Characterization of GM1 accumulation in synaptosomes

We characterized the GM1 accumulation in synaptosomes and non-synaptosomes using MβCD which can potently break down cholesterol- and GM1-rich DRMs such as lipid rafts by removing cholesterol. Synaptosomes and non-synaptosomes were prepared from whole brain minus hippocampus, cerebellum and the brainstem, and the hippocampus of two different age groups of mice (4-

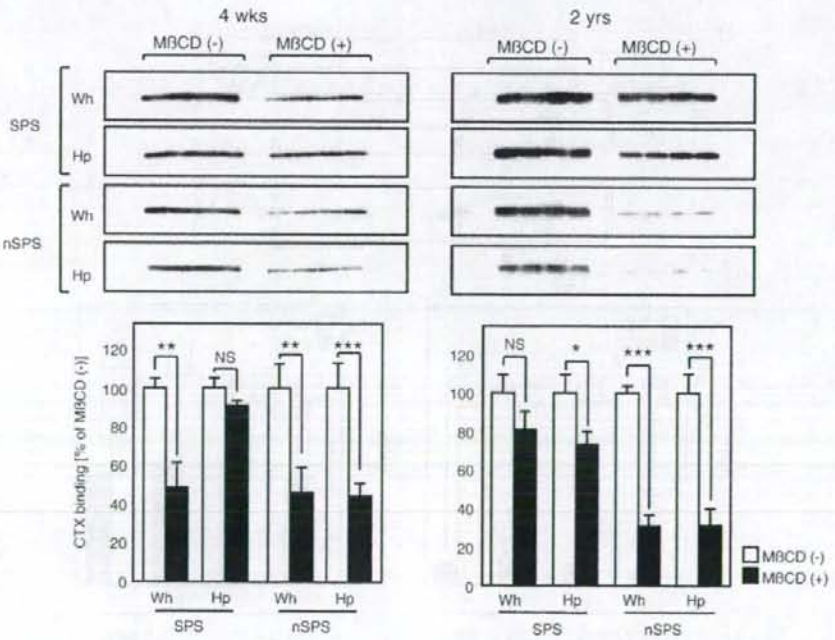

Fig. 2. GM1 accumulates in MβCD-treated synaptosomes prepared from aged mouse brain. The GM1 levels of synaptosomes and non-synaptosomes prepared from young (4-week-old) and aged (2-year-old) mouse brains with or without MβCD treatment are shown. Each lane of the blot contains 1 μg of synaptosomes or non-synaptosome protein prepared from mouse brain. The GM1 levels were determined by densitoscanning the blot following incubation with CTX-HRP. The intensities of the bands relative to those without MβCD treatment are indicated. Each column indicates the average of eight values±S.D. *$p<0.01$, **$p<0.001$, ***$p<0.0001$ (one-way ANOVA combined with Scheffe's test). SPS; synaptosome fraction, nSPS; non-synaptosome fraction, Wh: whole brain minus the hippocampus, cerebellum and brainstem, Hp: hippocampus.

week-old and 2-year-old). The GM1 levels in synaptosomes and non-synaptosomes, which were determined by the specific binding of CTX-HRP, were higher in the samples prepared from aged mouse brains than those from young mouse brains (Fig. 2). Notably, the GM1 accumulation in non-synaptosomes prepared from aged mouse brains markedly decreased following MβCD treatment whereas that in synaptosomes prepared from the same brains was resistant to MβCD treatment (Fig. 2). Although the extent of the GM1 accumulation was lower in the samples prepared from young mouse brains than from aged mouse brains, the resistance of GM1 accumulation to MβCD treatment was consistently observed in synaptosomes prepared from the hippocampus but not from the whole brain (Fig. 2). The levels of cholesterol markedly decreased in synaptosomes and non-synaptosomes from mouse brains of both age groups following MβCD treatment and the decrease in the levels of total phospholipids following MβCD treatment was moderate compared with that of cholesterol (data not shown).

To further characterize the resistance of GM1 showing age-dependent accumulation in the synaptosomes to MβCD treatment, we isolated DRM fractions from the synaptosomes and non-synaptosomes. The successful DRM isolation was confirmed by the observation of GM1 abundance in the fractions as was previously reported (Fig. 3A). We then compared the resistance of GM1 accumulation to MβCD treatment in each fraction between the synaptosomes and non-synaptosomes. Following MβCD treatment, the decrease in GM1 level in the DRM fractions prepared from synaptosomes (arrow a in Fig. 3B) was apparently less than that of the DRM fractions prepared from non-synaptosomes (arrow b in Fig. 3B). MβCD treatment markedly decreased the cholesterol levels, and the levels of total phospholipids also decreased following MβCD treatment but it was less than the decrease in cholesterol levels (Fig. 3B).

3.3. Aβ fibril formation in the presence of the synaptosomes or the DRMs prepared from synaptosomes

We determined whether the GM1 accumulation in the synaptosomes accelerates Aβ assembly into amyloid fibrils. We first incubated soluble Aβ in the presence of the synaptosomes prepared from three different age groups of mice (4-week-old, 1-year-old and 2-year-old groups). The ThT fluorescence intensity in the incubated mixtures increased in an age-dependent manner (Fig. 4A). Notably, the increase in ThT fluorescence intensity was significantly suppressed by coincubation with 4396C, an antibody specific to GAβ, suggesting that amyloid fibril formation in the presence of synaptosomes occurred through GAβ generation. We then incubated soluble Aβ1–40 in the presence of the synaptosomes or non-synaptosomes from aged mouse brain with or without MβCD pretreatment. The ThT fluorescence in

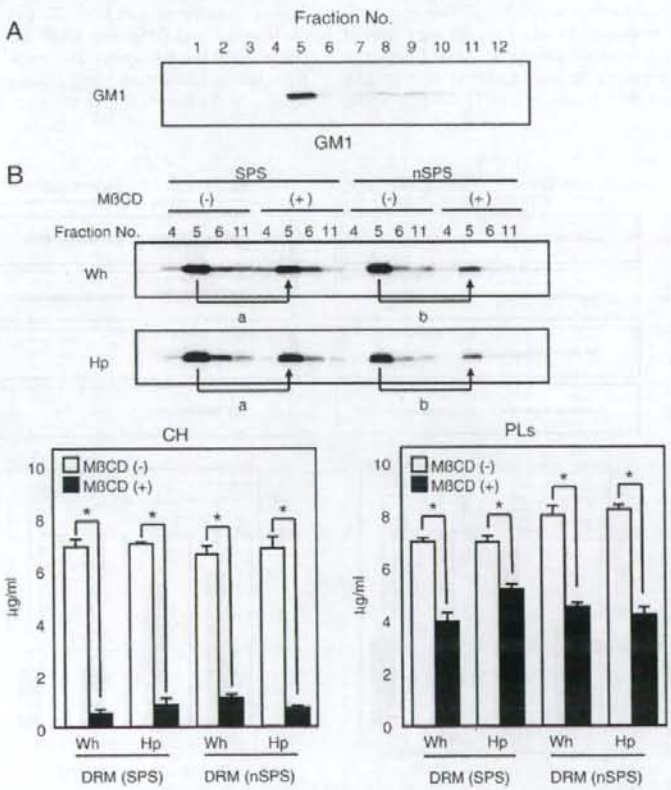

Fig. 3. GM1 accumulates in DRM isolated from MβCD-treated synaptosomes of aged mouse brain. (A) Fractions obtained by DRM isolation through sucrose density gradient fractionation were subjected to blot analysis using CTX-HRP. (B) The blot of DRM isolated from synaptosomes and non-synaptosomes prepared from aged (2-year-old) mouse brain with or without MβCD treatment, which was probed with CTX-HRP, is shown. The cholesterol (CH) and phospholipids (PLs) levels were determined using Determiner L and Phospholipids C, respectively. Each column indicates the average of three values±S.D. *$p<0.0001$ (one-way ANOVA combined with Scheffe's test). SPS; synaptosome fraction, nSPS; non-synaptosome fraction, Wh; whole brain minus the hippocampus, cerebellum and brainstem, Hp; hippocampus.